2016-07-01

Gas Phase Structure Characterization Using Fourier Transform Ion Cyclotron Resonance Mass Spectrometry

Anupriya Anupriya
Brigham Young University

Gas Phase Structure Characterization Using Fourier Transform Ion Cyclotron Resonance Mass Spectrometry

Anupriya

A dissertation submitted to the faculty of
Brigham Young University
in partial fulfillment of the requirements for the degree of

Doctor of Philosophy

David V. Dearden, Chair
Paul B. Farnsworth
Matthew C. Asplund
Daniel Austin
Roger Harrison

Department of Chemistry and Biochemistry

Brigham Young University

July 2016

ABSTRACT

Gas Phase Structure Characterization Using Fourier Transform
Ion Cyclotron Resonance Mass Spectrometry

Anupriya
Department of Chemistry and Biochemistry, BYU
Doctor of Philosophy

This dissertation investigates Fourier transform ion cyclotron resonance mass spectrometry (FTICR-MS) based techniques to study the impact of molecular structure on conformation and binding energetics. A novel method to determine collison cross sectional areas using FTICR (CRAFTI), initially developed by the Dearden lab, was applied to study the conformations of molecular systems with unique structural attributes in an attempt to explore the molecular range of CRAFTI. The systems chosen for CRAFTI studies include crown-ether alkylammonium complexes and biogenic amino acids. The results were found to be consistent with expected behavior, and strongly correlated with experimental measurements made using ion mobility spectrometry (IMS) and predictions from computations. The analytical sensitivity of CRAFTI was highlighted by its ability to distinguish the normal and branched structural isomers of butylamine. Besides conformation characterization, quantitative evaluation of binding was undertaken on metal ion-cryptand complexes on the FTICR instrument using sustained off-resonance irradiation –collision-induced dissociation (SORI CID) method. Complex formation and dissociation was found to be a strong function of both guest and host sizes which impacted steric selectivity, and polarizability. The results demonstrate the ability of FTICR to simultaneously determine structure, conformation and binding thereby providing comprehensive molecular characterization.

Keywords: FTICR-MS, CRAFTI, SORI-CID, Supramolecular complexes

ACKNOWLEDGEMENTS

The doctoral dissertation work presented in this thesis has been one of the most significant academic achievements of my life which could not have been possible without the support of the Almighty, family and friends. My first vote of thanks goes to my major advisor, Dr. David V. Dearden whose input and effort has been immeasurable. I would forever cherish his advice, guidance and support and constant encouragement. I am also grateful to my thesis committee members Dr. Paul B. Farnsworth, Dr. Daniel Austin, Dr. Roger Harrison and Dr. Matthew C. Asplund who gave critical inputs over the progress reports to provide direction and enhance the quality of my dissertation work. I am also indebted to the faculty members for providing an outstanding curriculum, enormous opportunities and financial support which have contributed towards my growth as a researcher.

Special thanks are due to my lab colleagues especially Dr. Fan Yang, who groomed me into the tools and techniques of routine research work. The collaborative work and intellectual discussions with Dr. Chad A. Jones and Ms. Jiewen Shen were also an enriching learning experience. I would also like to acknowledge the help of highly talented undergraduate students: Sam, Joslyn, Eluara, Conner and Brigham. I wish them a very bright future. No word of thanks can suffice for the stellar support role played by the departmental administrative staff.

I am also grateful to fellow graduate students and close friends for their support through thick and thin. I would especially like to communicate my gratitude to Dr. Anubhav Diwan, Dr. Swati Singh, Dr. Supriya Kanyal, Dr. Bhupinder Singh, Dr. Banrida Wahlang, Dr. Manali Agrawal, Antra and Prateek for all their care and affection. I would also like to mention the unconditional support of Dr. Saurabh Sarkar, who has been a close personal friend and has always stood by my side.

Finally, my education and this dissertation would not have been possible without the painstaking efforts and blessings of my family: my parents, Gopal Singh and Tara Dolia, my brother, Dr. Kamal Kishore and sister-in-law Neha. I would like to dedicate my dissertation to my family.

TABLE OF CONTENTS

TITLE PAGE i
ABSTRACT ii
ACKNOWLEDGEMENTS iii
TABLE OF CONTENTS v
LIST OF TABLES viii
LIST OF FIGURES ix
Chapter 1 Introduction 1
1.1 Background & Motivation 1
1.2 Historical overview of molecular conformation measurements 2
1.3 Current practice and its challenges 4
1.4 Thesis Objective & Outline 7
1.5 References 8
Chapter 2 Review: Structural characterization using FTICR-MS 11
2.1 Introduction 11
2.2 FTICR-MS 11
2.2.1 Principle: Ion motion inside ICR trapping cell 11
2.2.2 Ion excitation and detection in FTICR 15
2.2.3 FTICR instrumentation 17
2.3 Applications to structural characterization 22
2.3.1 Sustained off-resonance irradiation collision induced dissociation (SORI-CID) 22
2.3.2 Cross sectional Areas by FTICR-MS (CRAFTI) 26
2.4 References 32
Chapter 3 Conformational Analysis of n-Alkylamine Complexes with Crown Ethers Using FTICR "CRAFTI" Technique 37
3.1 Abstract 37
3.2 Introduction 37
3.3 Experimental 39
3.3.1 Materials 39
3.3.2 Instrumentation 40

3.3.3 Procedures 40
3.3.4 Computational cross section 41
3.4 Results and discussion 42
3.4.1 Experimental CRAFTI cross sections for crown ether-n-alkyl monoamine complex . 42
3.4.1.1 Variation in CCS as a function of crown ether ring size and alkyl monoamine chain length 42
3.4.1.2 CCS measurements of isomeric amines complexed with crown ethers 46
3.4.2 Comparison with IMS results 47
3.4.3 Comparison of CRAFTI cross section with cross sections computed using the exact hard sphere scattering method 49
3.4. Conclusion 52
3.5 References 52
Chapter 4 Collision Cross Sections for 20 Protonated Amino Acids: Fourier Transform Ion Cyclotron Resonance and Ion Mobility Result 57
4.1 Abstract 57
4.2 Introduction 58
4.3 Experimental 59
4.3.1 Materials 59
4.3.2 Instrumentation 59
4.3.3 Procedures 60
4.3.4 Computational Modeling 62
4.4 Results 62
4.4.1 Collision cross sections of protonated amino acids 62
4.5 Discussion 65
4.5.1 Structural information for protonated amino acids from cross sections 65
4.5.1.1 Compactness of protonated amino acids in the gas phase 67
4.5.1.2 Distinguishing isomeric and isobaric structures 68
4.5.2 Correlation of experimental cross sections with cross sections computed using the exact hard sphere scattering method 69
4.5.3 Correlation of CRAFTI cross sections with those from mobility methods 74
4.5.4 Disagreement of absolute CRAFTI cross sections with those from mobility methods 76

4.6 Conclusions 82
4.7 References 83
Chapter 5 Relative alkali metal binding strengths of cryptands in the gas phase using SORI-CID. 87
5.1 Abstract 87
5.2 Introduction 87
5.3 Experimental 88
5.3.1 Materials 88
5.3.2 Sample preparation 89
5.3.3 Instrumentation 89
5.3.4 Sustained off-resonance irradiation collision-induced dissociation experiments 89
5.3.5 Data analysis 91
5.4 Results 91
5.4.1 Electrospray of cryptands with alkali metals 91
5.4.2 Dissociation behavior of cryptand-alkali metal complexes 92
5.5 Discussion 95
5.6 Conclusions 97
5.7 References 98
Chapter 6 Summary and Perspective 102

LIST OF TABLES

Table 3.1 Cross sections (Å^2) for protonated crown ether-alkyl monoamine complexes using CRAFTI. 44

Table 3.2 Relative cavity sizes of crown ethers..... 45

Table 3.3 Cross sections (Å^2) of n- and t-butylamine with C4, C5 and C6..... 46

Table 3.4 Cross sections (Å^2) of protonated crown ether-alkyl monoamine complexes using Drift Ion mobility..... 48

Table 3.5 Cross sections (Å^2) of protonated crown ether-alkyl monoamine complexes using EHSS. 51

Table 4.1 Cross sections (Å^2) for protonated amino acids in various collision gases. 64

Table 4.2 Results for fits of experimental IMS and CRAFTI cross sections vs. cross sections calculated with the MOBCAL EHS method..... 72

LIST OF FIGURES

Figure 1.1 Schematic of a conventional drift time IMS system showing separation of three ions based on ion size. 6

Figure 2.1 Schematic of a cylindrical trapping cell composed of trapping, excitation and detection plates 13

Figure 2.2 Ion cyclotron motion exhibiting opposite movement for positive and negative ions..13

Figure 2.3 Schematic of 4.7 T FTICR mass spectrometer used in this work 20

Figure 2.4 Schematic of electrospray ionization..... 20

Figure 2.5 Focusing and guiding ion lenses in the Bruker FTICR mass spectrometer. 21

Figure 2.6 (a) Change in ion cyclotron radius (b) ion x-y trajectory as ions excite and de-excite due to difference between the excitation frequency and ion cyclotron frequency in SORI-CID..24

Figure 2.7 Change in FTICR linewidth for 18-crown-6•Cs^+ complex (inset) vs background Xe (a) Time domain signals over a range of Xe pressures (b) Power mode frequency domain spectra corresponding to the time domain transients of (a).(c) Full width at half maximum (FWHM) linewidths as a function of Xe number density, showing excellent linearity 27

Figure 2.8 Dependence of CRAFTI cross sections on (a) kinetic energy (determined using SF_6 collision gas) (b) Collison gas..... 29

Figure 3.1 Structures of the cyclic polyethers used in this study..... 41

Figure 3.2 Cross sections (Å^2) for protonated crown ether-alkyl monoamine complexes using CRAFTI 45

Figure 3.3 Correlation between CRAFTI cross section in argon and cross section from drift ion mobility 48

Figure 3.4 Correlation of experimental CCS measurements with Boltzmann-weighted CCS computed using the exact hard sphere (EHSS) scattering method from molecular models 50

Figure 4.1 Cross sections for 20 protonated amino acids computed using exact hard sphere scattering theory (EHS), and measured using CRAFTI in Ar at 1.9 keV in the lab frame or ion mobility spectrometry in N_2 with a 269 V cm^{-1} drift field, plotted as a function of molecular weight. 66

Figure 4.2 Correlation of experimental cross section measurements with Boltzmann-weighted cross sections computed using the exact hard sphere scattering method from molecular models. 71

Figure 4.3 Correlation of various protonated amino acid cross section data sets with ion mobility spectrometry (IMS) data measured in N_2 at a 269 V cm^{-1} drift field 75

Figure 5.1 Host ligands used in the study (a) dimethyloxacryptand [3.3.3] (b) dimethyloxacryptand [3.3.4] (c) cryptand [2.2.2] 90

Figure 5.2 Dissociation spectra of [dmo cryptand 333+Cs]$^+$ showing loss of neutral cryptand. . 93

Figure 5.3 SORI ion yield curves for [dmo cryptand 333+Cs]$^+$ complex. 93

Figure 5.4 SORI parent ion survival curve for metal-cryptand complexes as a function of average collision energy 94

Figure 5.5 Variation of dissociation threshold energy as a function of metal ion radius 94

Chapter 1 Introduction

1.1 Background & Motivation

The modern world is largely shaped by advances in chemical technology and new molecule development which in turn drive progress in myriad fields ranging from biopharmaceuticals to information technology. This makes holistic molecular characterization more important than ever before. Among other characteristics, molecular structure and dynamic 3D conformation can arguably be categorized to be critically important in determining properties and activity. For example, the physicochemical features of clinical drugs which determine transport to target tissues are well known to be affected by both shape and structure.[1] A number of protein complexes are responsible for diverse biological functions inside a human body.[2] If a protein fails to attain the folded native conformation, the unfolded protein or partially folded protein may combine to form amorphous aggregates which can give rise to a number of protein misfolding diseases.[3] If molecular conformation is adequately characterized, novel drugs could be screened for pharmacological activity at the biological receptor site thus helping with drug discovery. This background explains why a holistic molecular description, both structure and conformation, is of rapidly growing importance in the fields of chemistry and medicine.

While the field of structural determination forms the cornerstone of analytical chemistry through innumerable techniques used on a routine basis, conformational determination is a relatively less widespread practice and presents a dynamic field of research. Comprehensive molecular characterization with specific emphasis on molecular conformation characterization and its impact on molecular binding in a biochemical context is the central focus of this dissertation.

1.2 Historical overview of molecular conformation measurements

Traditionally, classical techniques like X-ray diffraction (XRD)[4] and nuclear magnetic resonance (NMR)[5] are used to provide structural information from which conformation can be predicted. However, biomolecules are often not readily crystallized, often limiting the XRD approach. Additionally, the biological activity is influenced by dynamic conformation at the target site, which is not necessarily the same as predicted from solid state crystal structure. Biological systems are indeed complicated and the native conformation is dictated by local conditions; most importantly bio fluids, other solutes and temperature. The impact of the chemical nature of the local solvent must be accounted for, and other effects like solution ionization based on pH sensitivity, solvation power etc. must also be considered. NMR studies require a large amount of sample (commonly hundreds of milligrams), limiting the application of NMR to samples available in smaller quantities. These complexities make NMR analysis very challenging for conformation analysis. Mass spectrometry (MS) based techniques like H/D exchange[6] and gas-phase proton transfer reactions[7] are indirect and provide less detailed information compared to X-ray or NMR.

Modern analyses frequently use collision cross section (CCS) as the preferred molecular conformation descriptor as it conveys direct information about the shape and size of the molecule. CCS is defined as the area around an analyte particle in which the center of another particle (like a collision gas molecule) must be in order for a collision to occur. Thus, collision of an ion with a neutral gas reflects ion size and can provide useful conformational information. Furthermore, CCS determinations can be compared and validated against theoretical *in silico* predictions or other complimentary techniques.[8]

Gas phase CCS determinations can identify accurate conformation in the absence of any interfering solvent and matrix effects so that the binding site chemistry can be better understood.

Model host-guest systems used in supramolecular chemistry, characterized through CCS determinations, convey great information about the net effect of weak non-covalent interactions, and general principles of size and shape complementarity. Another advantage of using gas phase studies is the ease of comparison with each other for different supramolecular systems, which is difficult to achieve for solution- or solid state-based studies.[9] The dynamic quantitative understanding of how structure and conformation influence physiochemical properties and biochemical activity is a key first step to understanding extremely complicated biochemical ligand-receptor chemistry.

In the early 1960s, collision cross sections were measured for several ions from the linewidths of ion cyclotron resonance spectra.[10] The collisional broadening of the ICR line width was attributed to ion-molecular interactions and inelastic collisions by Beauchamp et al. Elastic collisions between ion and neutral with or without charge transfer and the presence of single isotopes or mixtures were some of the cases explored in the study. They also described the influence of external parameters, such as temperature, pressure and electric field, on the ICR line shape.[13] Later, mobilities of H^+, H_3^+, Na^+ and similar ions were measured in methane and hydrogen based on the collisional broadening phenomenon in ICR.[11] The results obtained in this study agreed well with drift tube measurements. The study also found that line width varied linearly with the pressure of the neutral gas. Widespread application of the drift ICR method was never realized due to its inherent drawbacks of lower mass resolution and the need for multiple low energy collisions.

In 1993, Covey and Douglas[10] introduced a novel method for determination of collision cross sections of biomolecules based on an energy loss method. Ions are injected into a radiofrequency quadrupole and collide with the neutral gas upon passage through the collision cell. With application of a hard sphere model, the average kinetic energy loss per collision is calculated

and is used to determine the number of collisions and consequently the collision cross section. This study reported cross sections for ions formed from motilin, cytochrome c, myoglobin, ubiquitin and bovine serum albumin. The method was further modified and the results from this diffuse scattering method were found to be within 5% of the ion mobility experiments.

1.3 Current practice and its challenges

Though ion mobility mass spectrometers (IMMS) were introduced in 1962,[12] their stature in conformation measurement has progressively risen to be the current gold standard. In principle, an ionized sample is introduced into a drift tube filled with buffer gas and gaseous ions are accelerated under the influence of a weak electric field (Figure 1.1). Low energy collisions occur between the ion and the buffer gas (low vacuum or atmospheric pressure conditions). Ions with higher cross section suffer more collisions, and consequently exhibit a longer drift time across the tube. Further, separated ions with different drift velocities pass through a mass analyzer and such coupling helps achieve separation according to size, shape and charge of the ion by IMMS.[13] In the low-field limit, the collision cross section, σ_{avg} can be calculated using mobility by Equation 1-1.[14]

$$\sigma_{avg} = \frac{(18\pi)^{1/2}}{16}\left[\frac{1}{m_i}+\frac{1}{m_b}\right]\frac{ze}{(k_bT)^{1/2}}\frac{t_dE}{L}\frac{760}{P}\frac{T}{273.2}\frac{1}{N_o} \qquad (1\text{-}1)$$

Here, m_i is the mass of the ion, m_b is the mass of the buffer gas, z is the charge of the ion, k_b is the Boltzmann constant, t_d is the drift time, E is the electric field strength, T is the temperature, N_o is the number density of the collision gas, P is the pressure of the collision gas and L is the drift tube length.

There are some drawbacks to using IMMS for measuring collision cross section. First, there is a need to calibrate the instrument before every use as the temperature and pressure have consequential roles in determining the collision cross section.[15] Second, migration through the drift tube involves multiple collisions of the ions with the buffer gas which may impact the conformations of the system under study.[16] Lastly, IMMS requires a specifically designed instrument to carry out such measurements.

CRAFTI (cross sectional areas by Fourier transform ion cyclotron resonance) is a novel technique for measuring CCS using Fourier transform ion cyclotron resonance mass spectrometry (FTICR-MS).[17] In principle, it measures cross sections for collisions of gas phase ions with neutral background gas by measuring signal decay as ions are scattered out of a coherent ion packet. CRAFTI promises to provide a complementary technique that can be performed on any FTICR-MS with minimal modification. This provides a great advantage as one FTICR instrument could be used to determine the structure, conformation and binding characteristics. However, more optimization studies are needed before CRAFTI can be routinely applied for conformation determination.

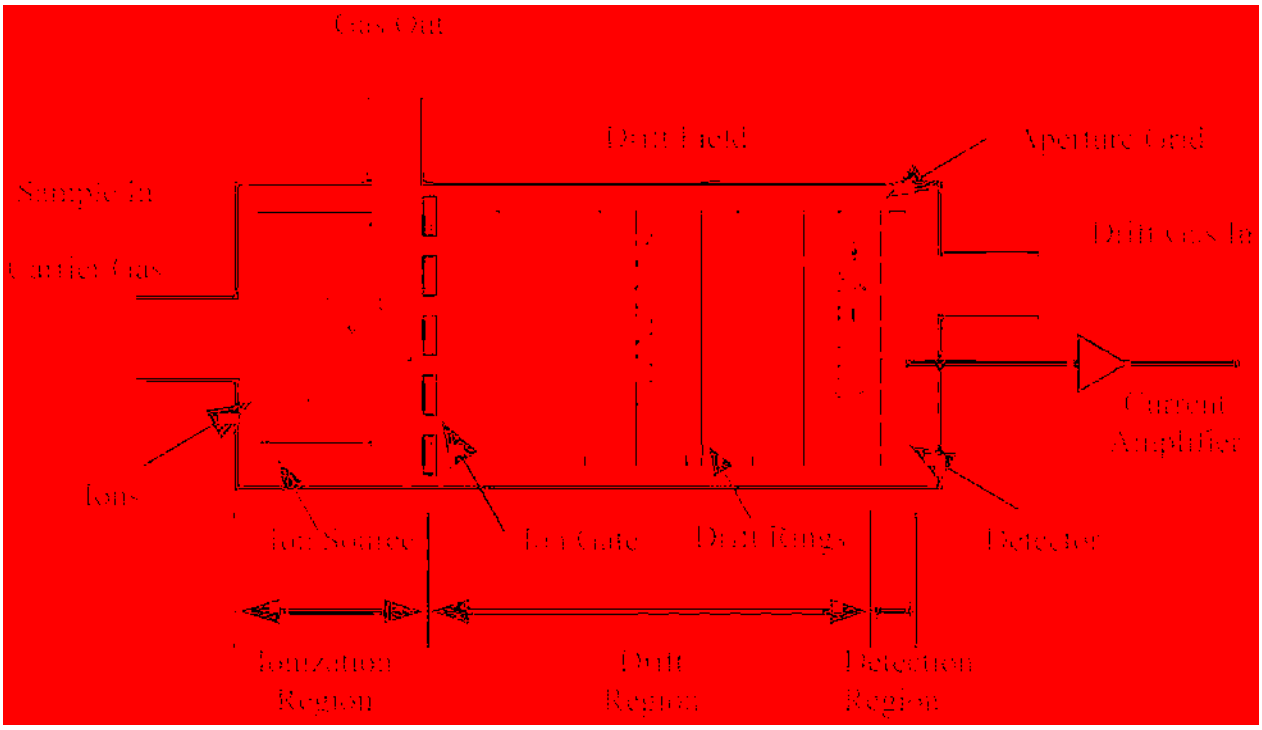

Figure 1.1 Schematic of a conventional drift time IMS system showing separation of three ions based on ion size. *(Reprinted with permission from "Review on Ion Mobility Spectrometry. Part 1: current instrumentation" by Gracia I et al., 2014, Analyst, 1376-1390, copyright (2014) The Royal Society of Chemistry)*

1.4 Thesis Objective & Outline

CRAFTI method optimization through characterization of different biosimilar host-guest complexes is described in this dissertation. These CRAFTI studies are directed towards realizing the primary objective of holistic molecular characterization through gas phase molecular conformation and binding studies. The methodological flow and schematic studies are presented in the dissertation through the following chapters:

Chapter 2 provides a detailed introduction and review to FTICR-MS and its application towards determining molecular conformation and binding energetics. **Chapter 3** presents the experimental results for characterization of well-known crown ether ammonium complexes and comparison with other experimental and computational determinations. CRAFTI results to characterize molecular shapes of 20 naturally occurring amino acids are presented in **Chapter 4**. **In Chapter 5,** a method to characterize the binding of supramolecular complexes (dimethyloxacryptands [3.3.3] and [3.3.4]) is investigated. **Chapter 6** summarizes the important conclusions from these studies and identifies areas of further research.

1.5 References

1. van de Waterbeemd, H.; Smith, D. A.; Beaumont, K.; Walker, D. K., Property-based design: optimization of drug absorption and pharmacokinetics. *J. Med. Chem.* **2001,** *44* (9), 1313-1333.

2. Nooren, I. M.; Thornton, J. M., Diversity of protein–protein interactions. *EMBO* **2003,** *22* (14), 3486-3492.

3. Chiti, F.; Dobson, C. M., Protein misfolding, functional amyloid, and human disease. *Annu. Rev. Biochem.* **2006,** *75*, 333-366.

4. Bhattacharya, A. A.; Grüne, T.; Curry, S., Crystallographic analysis reveals common modes of binding of medium and long-chain fatty acids to human serum albumin. *J. Mol. Biol* **2000,** *303* (5), 721-732.

5. Choi, J.-K.; Ho, J.; Curry, S.; Qin, D.; Bittman, R.; Hamilton, J. A., Interactions of very long-chain saturated fatty acids with serum albumin. *J. Lipid Res.* **2002,** *43* (7), 1000-1010.

6. Freitas, M. A.; Hendrickson, C. L.; Emmett, M. R.; Marshall, A. G., Gas-phase bovine ubiquitin cation conformations resolved by gas-phase hydrogen/deuterium exchange rate and extent. *Int. J. Mass spectrom.* **1999,** *185*, 565-575.

7. Valentine, S. J.; Counterman, A. E.; Clemmer, D. E., Conformer-dependent proton-transfer reactions of ubiquitin ions. *J. Am. Soc. Mass Spectrom.* **1997,** *8* (9), 954-961.

8. Knapman, T. W.; Berryman, J. T.; Campuzano, I.; Harris, S. A.; Ashcroft, A. E., Considerations in experimental and theoretical collision cross-section measurements of small

molecules using travelling wave ion mobility spectrometry-mass spectrometry. *Int. J. Mass spectrom.* **2010,** *298* (1), 17-23.

9. Dearden, D. V.; Liang, Y.; Nicoll, J. B.; Kellersberger, K. A., Study of gas-phase molecular recognition using Fourier transform ion cyclotron resonance mass spectrometry (FTICR/MS). *J. Mass Spectrom.* **2001,** *36* (9), 989-997.

10. Beauchamp, J., Theory of Collision-Broadened Ion Cyclotron Resonance Spectra. *J. Chem. Phys.* **1967,** *46*, 1231.

11. Ridge, D.; Beauchamp, J., The interaction of ions with nonpolar neutrals: The collision broadening of ion cyclotron resonance lines of ions in hydrogen and methane. *J. Chem. Phys.* **1976,** *64*, 2735.

12. McDaniel, E.; Martin, D.; Barnes, W., Drift tube-mass spectrometer for studies of low-energy ion-molecule reactions. *Rev. Sci. Instrum.* **1962,** *33* (1), 2-7.

13. Clemmer, D. E.; Jarrold, M. F., Ion mobility measurements and their applications to clusters and biomolecules. *J. Mass Spectrom.* **1997,** *32* (6), 577-592.

14. Covey, T.; Douglas, D., Collision cross sections for protein ions. *J. Am. Soc. Mass Spectrom.* **1993,** *4* (8), 616-623.

15. Smith, D. P.; Knapman, T. W.; Campuzano, I.; Malham, R. W.; Berryman, J. T.; Radforda, S. E.; Ashcrofta, A. E., Deciphering drift time measurements from travelling wave ion mobility spectrometry-mass spectrometry studies. *Eur J Mass Spectrom* **2009,** *12* (13), 13.

16. Merenbloom, S. I.; Flick, T. G.; Williams, E. R., How hot are your ions in TWAVE ion mobility spectrometry? *J. Am. Soc. Mass Spectrom.* **2012,** *23* (3), 553-562.

17. Yang, F.; Voelkel, J. E.; Dearden, D. V., Collision cross sectional areas from analysis of fourier transform ion cyclotron resonance line width: a new method for characterizing molecular structure. *Anal. Chem.* **2012,** *84* (11), 4851-4857.

Chapter 2 Review: Structural characterization using FTICR-MS

2.1 Introduction

Mass spectrometry (MS) has a critical and often indispensable role in modern molecular identification and quantification. In principle, a molecule is ionized and collisionally activated to produce an ion with internal energies sufficient to lead to fragmentation. The chemical linkages in the parent molecule dictate the nature and stability of the fragments produced, which are detected and analyzed according to their mass-to-charge (*m/z)* ratio. Within this generic MS methodology, many different techniques are used depending upon modes of ion excitation, detection and analysis. The current chapter focuses on reviewing one of the most frequently used techniques, Fourier transform ion cyclotron resonance mass spectrometry (FTICR-MS). FTICR-MS has advantages of high mass measuring accuracy (sub ppm), sensitivity (subattomole detection), ultrahigh resolving power and tandem MS^n capabilities.[1] This review specifically focuses on how FTICR-MS can be used to provide information on molecular conformation and binding energetics.

2.2 FTICR-MS

2.2.1 Principle: Ion motion inside ICR trapping cell.

The trapping cell is the heart of an FTICR mass spectrometer. Figure 2.1 presents a schematic of a cylindrical trapping cell, where ions undergo three different types of ion motions: cyclotron motion, trapping oscillation and magnetron motion.

Cyclotron motion. When an ion with a mass m, charge q, and velocity v, moves through a spatially homogenous magnetic field, it experiences an inward force known as the Lorentz force, **F,** given by Equation 2-1:

$$\mathbf{F} = q\mathbf{v} \times \mathbf{B} \qquad (2\text{-}1)$$

This force drives the ion into a circular motion perpendicular to the plane of the magnetic field (Figure 2.2). This centripetal force is balanced by an outward directed centrifugal force which stabilizes the ion orbit such that

$$q v_{xy} \boldsymbol{B} = \frac{m v_{xy}^2}{r} \tag{2-2}$$

The angular velocity, ω, about the z-axis, is given by:

$$\omega = \frac{v_{xy}}{r} \tag{2-3}$$

Combining Equation 2-2 and 2-3, the "unperturbed" ion cyclotron frequency, ω_c is given by:

$$\omega_c = \frac{q\boldsymbol{B}}{m} \tag{2-4}$$

Equation 2-4 highlights an inverse relationship between ion's *m/z* ratio and its cyclotron frequency. Hence, measuring an ion's cyclotron frequency helps determine its *m/z* ratio and which is independent of ion velocity. Typically, the cyclotron frequencies of ions range from ten kHz to hundreds of kHz, which can be easily determined by commercially available electronics.

Trapping oscillations. Ions enter the trapping cell along the direction of magnetic field (z-direction) and are effectively trapped by applying a small voltage across the two trapping plates which prevents ion ejection along the z-axis. This causes the ions to undergo a harmonic oscillation orthogonal to the cyclotron motion, termed trapping oscillation.

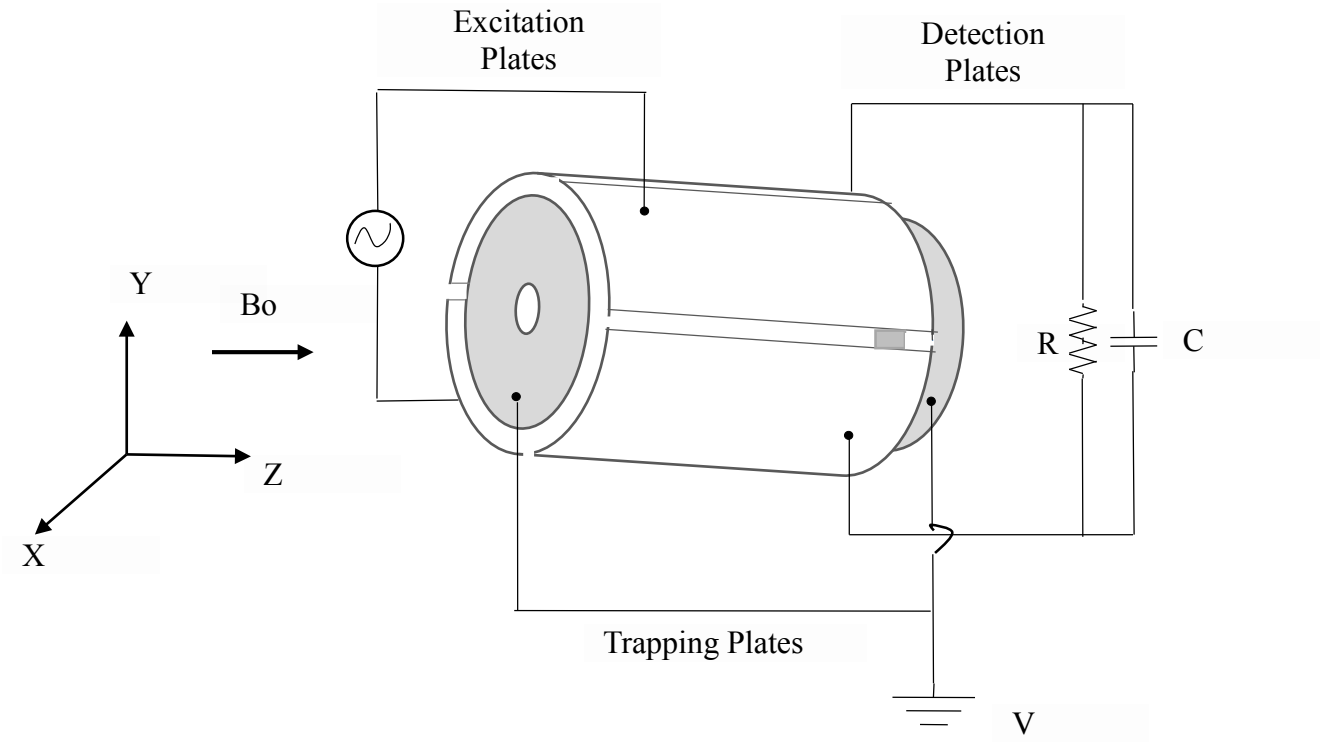

Figure 2.1 Schematic of a cylindrical trapping cell composed of trapping, excitation and detection plates

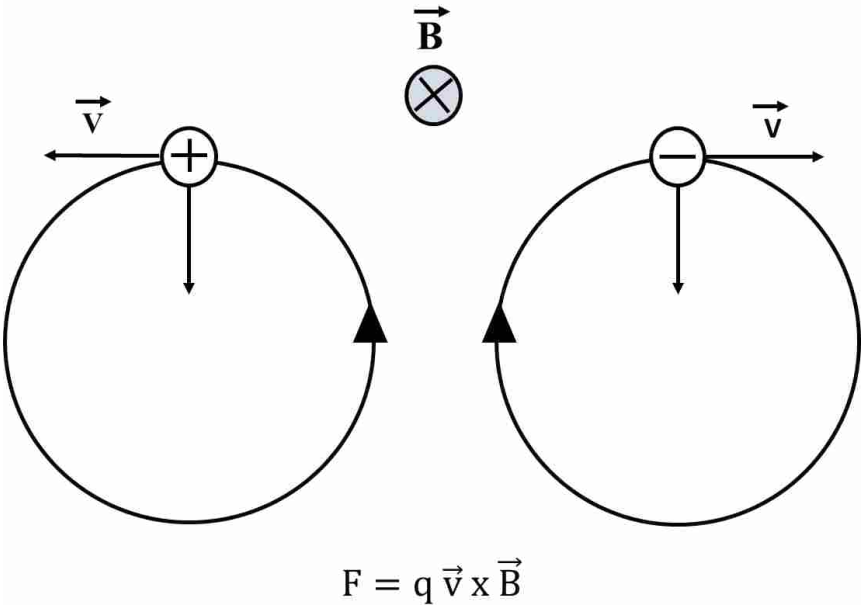

Figure 2.2 Ion cyclotron motion exhibiting opposite movement for positive and negative ions

It is given by Equation 2-5:

$$\omega_z = \sqrt{\frac{2qV\alpha}{ma^2}} \tag{2-5}$$

In the above Equation, V is the trapping potential, α is the geometric factor of the cell, and a is the z-axis length of the cell. Typically, the trapping oscillation frequency is tens of kHz.

Magnetron motion. The last fundamental motion in an ICR trapping cell is called magnetron motion, which arises from interactions of the ion with the magnetic field and the radial component of the electric field. The radial electric field induces an electrostatic force on the ion opposite to the direction of the Lorentz force. Hence the total force ($\boldsymbol{F}_{total}$) acting on an ion is given by Equation 2-6:

$$\boldsymbol{F}_{total} = m\omega^2 r - q\boldsymbol{B}\omega + \frac{qV\alpha}{a^2} r \tag{2-6}$$

The solutions to the above quadratic equation are given by:

$$\omega_+ = \frac{\omega_c}{2} + \sqrt{\left(\frac{\omega_c}{2}\right)^2 - \frac{\omega_z^2}{2}} \tag{2-7}$$

$$\omega_- = \frac{\omega_c}{2} - \sqrt{\left(\frac{\omega_c}{2}\right)^2 - \frac{\omega_z^2}{2}} \tag{2-8}$$

Equation 2-7 calculates the reduced cyclotron frequency or the ion's real cyclotron frequency, ω_+ while Equation 2-8 calculates the magnetron frequency, ω_-, where ω_z is the trapping oscillation. The magnetron frequency is minor in comparison to the cyclotron frequency and is usually neglected without introducing significant error.

2.2.2 Ion excitation and detection in FTICR

From Equation 2-4, it is known that the ion cyclotron frequency can be converted to give the ion's *m/z*. This cyclotron frequency is ascertained from the image current produced by the orbiting ions on detection plates. Initially the ions' orbital radii are small and ions are randomly distributed giving a net zero detectable image current. Upon application of a radio frequency (rf) pulse to the excitation plates, the ions attain spatial coherence and accelerate to larger orbits when the excitation frequency is in resonance with the ion's cyclotron frequency. The final radius of the ion packet is given by:

$$r = \frac{E_{ex}t}{2B} \tag{2-9}$$

In the above equation E_{ex} is the rf voltage applied across the excitation plates, t is excitation time and B is the magnetic field strength. As is apparent from Equation 2-9 the orbit radius achieved by the ions is independent of the *m/z* of the ions. Hence, all the ions can be excited to the same orbit radius under constant excitation conditions. The ion coherent motion damps slowly under low pressure conditions due to collisions with the background neutral or coupling to the excitation/detection electronics. The oscillating image current is induced on the detect plates by the coherently rotating ion packet. This signal is further amplified and digitized to give a time domain signal. This time domain signal upon Fourier transformation produces a frequency domain signal that can be converted to a mass spectrum using Equation 2-4.

Several types of excitation pulses can be employed depending on the end goal. The most commonly used among them is the 'chirp excitation' which provides a broadband excitation of the range of *m/z* ratios desired.[2]

A linear chirp waveform is described by Equation 2-10:

$$f(t) = f(0) + kt \tag{2-10}$$

Here *f(t)* and *f(0)* are the frequency at time t and 0 respectively and *k* is the chirp rate that depicts the rate of change of the frequency sweep. This kind of excitation is non selective, exciting all the ions in the excited frequency range, and has an advantage of easy execution. The 'stored waveform inverse Fourier transform excitation'(SWIFT) also offers a broadband mass-selective excitation, providing better command over the excitation characteristics.[3] A SWIFT excitation is based on the principle of specifying a desired excitation magnitude spectrum whose equivalent time-domain spectrum is then generated using inverse Fourier transformation. It is a more sophisticated approach as it permits a uniform excitation over a range of masses and lends higher selectivity to the excitation-ejection process. The 'single frequency excite' is the simplest excitation event. In this technique, ions are excited by applying an rf pulse resonant with the trapped ions' cyclotron frequency. The ion radius expands as the ion absorbs energy and is given by Equation 2-11:

$$r = \frac{\beta V_{p-p} T_{excite}}{2dB} \tag{2-11}$$

Here β is a geometry factor for the trapping cell, $V_{p\text{-}p}$ is the peak-to-peak amplitude of the applied voltage, T_{excite} is the length of the rf pulse, d is the diameter of the cell and B is magnetic field strength. The kinetic energy of an ion post excitation with a single frequency event can be calculated using Equation 2-12 below:

$$KE_{(post\ excitation)} = \frac{1.20607\times10^{7}\beta^{2}z^{2}V_{p-p}T_{excite}}{d^{2}m} \tag{2-12}$$

A combination of excite and detect event, the simultaneous excite/detect event (SED), allows real time observation of the coherent ion packet[4] and is employed in the CRAFTI technique

described later.[5] It also has a diagnostic advantage where it allows detection of the excite rf pulse directly using detection plates.

2.2.3 FTICR instrumentation

A schematic of the 4.7 T FTICR mass spectrometer used in this work is shown in Figure 2.3. Like other mass spectrometers, FTICR-MS consists of the following vital components: ionization source, ion guide optics, analyzer (previously described) and magnet.

Ionization source. One of the first steps in FTICR-MS is creation of gas phase ions. This can be accomplished using either internal or external ion sources. Internal ion sources allow molecules to be ionized inside the cell by introducing neutrals directly into the trap using a leak valve or probe. External ion sources generate ions outside of the ICR cell and ions are transmitted to the cell through a series of ion guide optics and regions of differential pumping.

Internal ion source. A classic example of internal ion source is 'electron impact' (EI), which is one of the earliest methods of ionization introduced by Dempster in 1918.[6] It is a "hard" ionization technique i.e. it causes the ions to fragment and employs a high energy electron beam (~70 eV) to remove valence electron from a molecule (producing a positive ion) or a low energy beam to allow capture of an electron (yielding a net negative charge) inside the cell. Due to the excess energy provided by the method, multiple fragmentations of the molecule can take place. Samples of high volatility can be introduced by means of inserting a container into a sealed port from which a leak valve allows the neutrals to directly enter the cell. Nonvolatile components are often inserted on heated probes and vaporized. An internal EI source, which generates background Ar^+ ions for pressure measurement, is employed for CRAFTI.[7]

External ion source. External ionization techniques generally provide softer ionization (though external EI sources are also available) and can be used for non-volatile, thermally unstable

molecules. Electrospray ionization (ESI) is one of the most common ionization techniques, introduced by John Fenn.[8] The ESI phenomenon can be divided into three major steps: formation of charged droplets, reduction in droplet size, and creation of desolvated ions (Figure 2.4). The ESI capillary acts as the working electrode while the parallel plate acts as a counter electrode typically kept a distance of 0.1 to 2 cm apart. A high voltage of ± 2-5 kV is applied between them. ESI can be operated in either positive or negative mode, where the capillary voltage is kept positive or negative respectively allowing opposite electrophoretic movement for cations and anions. When the ions at the capillary tip interact with the applied electric field, solution is drawn from the surface to form a 'Taylor cone'.[9] Meanwhile, when there is enough charge density at the tip of the cone, a charged droplet leaves in the direction of the electric field overcoming the opposing surface tension of the solution. Solvent evaporation during the transport of charged droplets through the electric field leads to increased electrostatic repulsion culminating in coulombic fission. Several factors that affect the ion charge are: applied voltage, the pH of the solution, the solvent used and its polarity and addition of cations or anions.[10]

Ion accumulation and Ion optics. While travelling from atmospheric pressure ion sources to the mass analyzer, ions are exposed to differential pumping conditions and are guided by ion optics. Ions from the heated metal capillary reach a set of skimmers that remove excess neutrals and help the ions accumulate. All the ions with diverse kinetic energy gather in the succeeding hexapole where a trapping voltage is applied for 500 to 2000 ms. This makes all the ions concentrate and acquire more uniform kinetic energy. Subsequently, the accumulated ions are ejected from the hexapole and pass through a stack of electrostatic lenses including *Einzel* lenses, which guide the ions to the analyzer cell (Figure 2.5). All the hollow cylindrical lenses PL1, PL2, PL9, FOCL1 and FOCL2 are focusing lenses which help focus the ion beam. DPL2 and DPL4

further help to deflect the ion beam along the vertical (y) and horizontal (x) directions respectively. Under the influence of high voltage (HVO), ions are accelerated to several thousands of eV energy. The split cylinders XDFL and YDFL guide the ions into place by deflecting in the x and y directions respectively.

Magnet. Magnetic field strength in FTICR-MS is provided by superconducting solenoid magnets. They are capable of generating much higher field strength than conventional electromagnets, without any power supply. Uninterrupted operation of the magnet is ensured by maintaining a sufficiently low temperature that keeps the solenoid magnet in a superconducting state. This is achieved by using liquid helium as a coolant. In order to prevent liquid helium from boiling off, relatively less expensive liquid nitrogen fills the outer jacket surrounding the magnet coils and the liquid helium. There is dramatic increase in the quality of the ion signal as the magnetic field strength, **B,** in FTICR is increased. This could be attributed to: a) a linear relationship between the magnetic field and the mass resolving power, b) an inverse relationship of the magnetic field strength with the time required for data acquisition and initial ion radius, c) upper mass limit, post excitation kinetic energy and time period for ion entrapment increases with B^2.[11] This has led to modern FTICR-MS instruments being operated at strengths up to 21 T,[12] which is a significant improvement over their predecessors, which operated at 1.4 T in the 1960s.[13] As superconducting magnets provide homogenous magnetic field strength, a larger magnetic bore diameter is possible, which increases the dynamic range of the instrument.

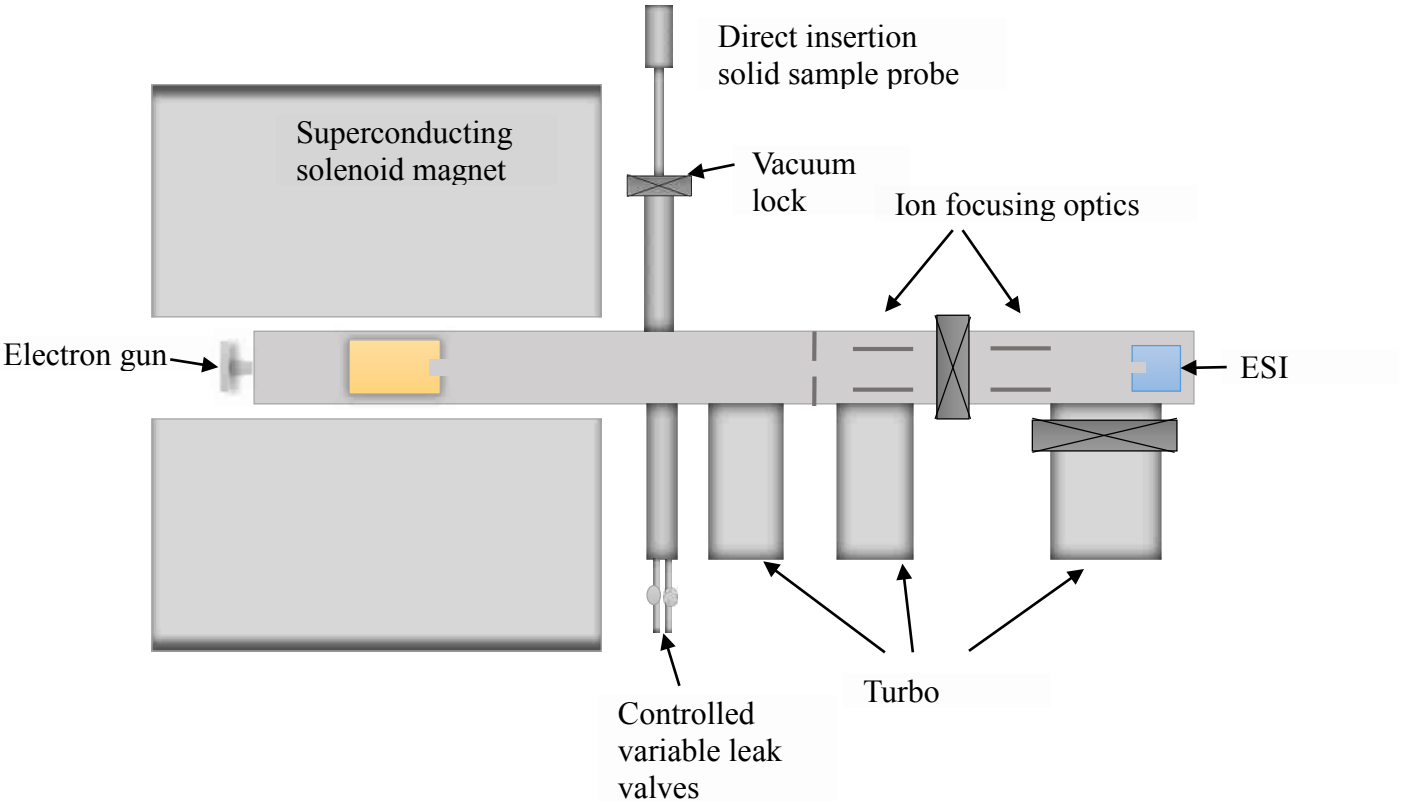

Figure 2.3 Schematic of 4.7 T FTICR mass spectrometer used in this work

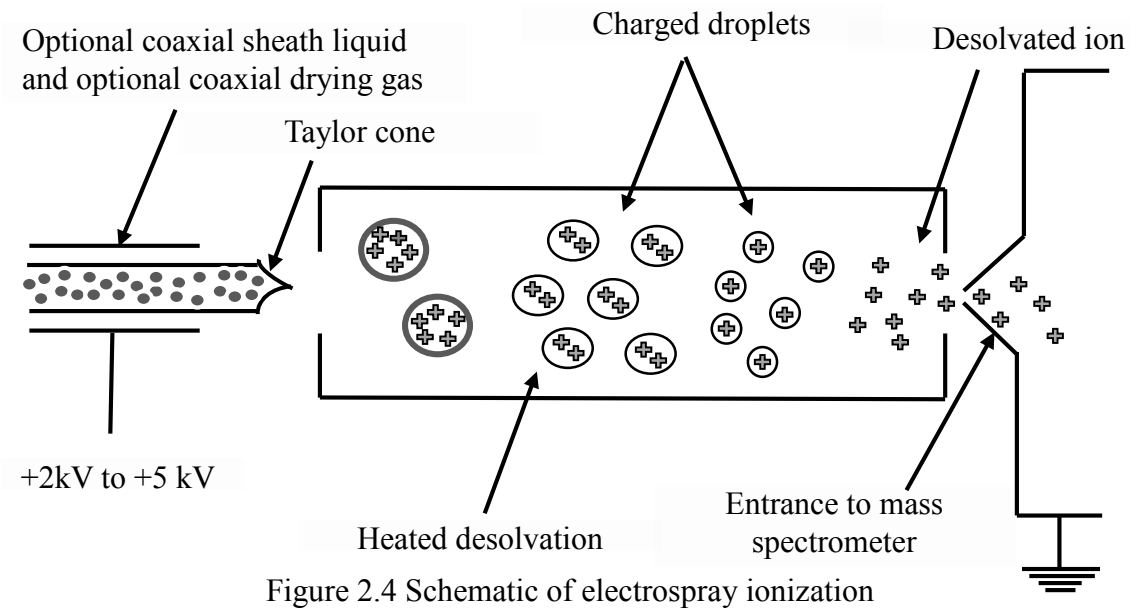

Figure 2.4 Schematic of electrospray ionization

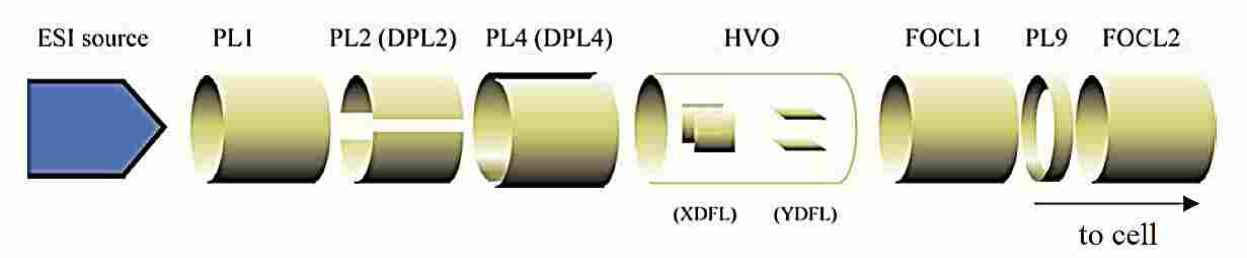

PL1, PL2, PL4, PL9- Optic plates

HVO- High Voltages

XDFL- X-Deflector

YDFL –Y-Deflector

FOCL1, FOCL2 – Focusing Lenses

Figure 2.5 Focusing and guiding ion lenses in the Bruker FTICR mass spectrometer.

(Reprinted with permission from Contreras, C.S. 2008. Carbohydrates and Amino Acids: Infrared Multiple Photon Dissociation Spectroscopy and Density Functional Theory Calculations. Ph.D. dissertation (Page 66, Figure 2-8) University of Florida, Gainesville, Florida.)

2.3 Applications to structural characterization

Since its inception in 1974 by Marshall and Comisarow,[13] more than 800 FTICR-MS have been installed in laboratories worldwide.[14] The most common application is structural elucidation using tandem MS/MS techniques. Conventional applications for FTICR-MS have been thoroughly reviewed several times.[15] The current review focuses on specific application towards (a) binding energetics through SORI-CID and (b) characterization of conformation through CRAFTI.

2.3.1 Sustained off-resonance irradiation collision induced dissociation (SORI-CID)

FTMS offers tandem-in-time experiments where ion selection is followed by dissociation within the same space. Dissociation within the ICR cell is accomplished by inelastic collisions with non-reactive neutral target molecules. Dissociation occurs due to reduced path length (at pressures elevated above the background pressure of the instrument) and increased ion velocity. Ionic excitation within FTMS is practiced with mainly two methodologies: resonant excitation (RE) or sustained off-resonance irradiation (SORI) excitation.[16] In the RE method, an rf pulse is applied at the exact cyclotron frequency of the ion which results in an increased orbital radius (r) of a precalculated value. The maximum translational energy (E_{tr}) that could be achieved is given by Equation 2-13:[17]

$$E_{tr} = \left(\frac{E}{\sqrt{2}}\right)^2 \frac{e^2 t^2}{8m} \qquad (2\text{-}13)$$

Where E is the electric field amplitude, e is the electric charge, t is the duration of the electric field pulse and m is the mass of the ion. While this is conceptually straightforward, this approach has several practical limitations. A major drawback is the excess internal energy resulting from resonant collisions under single collision conditions, which allows access to multiple decomposition pathways. This results in a complicated spectrum that is often difficult to

deconvolute. If multiple collision conditions occur, dissociation of high mass ions is restricted due to the radial and diffusional loss of product ions. This could also lead to significant distortion of the ion cloud, ultimately resulting in lowered mass resolution and shorter transients.[16] Lastly, method optimization could be quite instrument sensitive and time consuming.

In contrast to RE, SORI-CID principally operates on sampling the lowest decomposition pathways as the excess energy is gradually deposited into the ions and rapidly randomized within the cell without ejection. In principle, ions are irradiated with a single off resonant sine wave excitation pulse (above or below the resonant frequency of the precursor ion) in the presence of a background gas pressure which could be elevated up to 10^{-5} mbar. Consequently, the kinetic energy of the ions oscillates with time (Figure 2.6) leading to random collisions. To achieve optimum conditions, the collision frequency should be high enough to sample the required kinetic energy range and low enough to prevent dampening of the ion's kinetic energy. An excitation pulse longer than the time between collisions ensures multiple sequential low energy collisions, which slowly heat the ions to increase their internal energy inducing dissociation by means of lowest energy fragmentation pathway. Ever since its initial conception, this technique has found many applications in biopolymers such as proteins,[18] peptides,[19] oligonucleotides[20] as well as supramolecular chemistry.[21]

To compare SORI data among different molecular complexes, a quasi–quantitative approach was proposed by Zhang et.al.[22] As SORI deposits energy by multiple low energy collisions, the relative energy available for dissociation of a precursor ion, $E_{SORI,}$ is a function of both the average collision energy and total number of collisions. An expression was derived for the amount of energy deposited in the ion via a SORI event (Equation 2-14):[22]

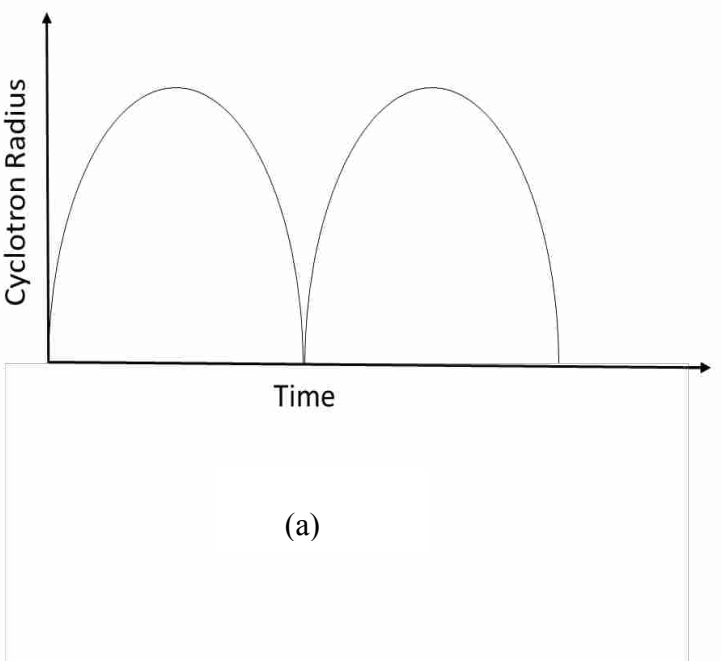

(a)

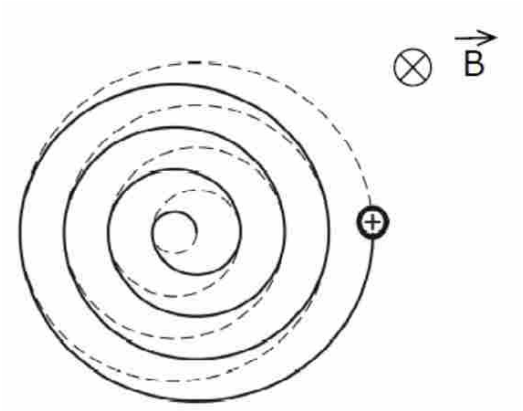

(b)

Figure 2.6 (a) Change in ion cyclotron radius (b) ion x-y trajectory as ions excite and de-excite due to difference between the excitation frequency and ion cyclotron frequency in SORI-CID. (*Adapted* with permission *from "Stored waveform inverse Fourier transform (SWIFT) ion excitation in trapped-ion mass spectrometry: Theory and applications" by Guan SH and Marshal AG,* 1996, *Int. J. Mass Spectrom. Ion Processes*, 5-37. copyright (1996) Elsevier Science B.V.)

$$E_{SORI} = N^{*}\sigma K_v f_E t_{coll} \frac{\beta^3 q^3}{128\pi^3 d^3 (\Delta f)^3} \left(\frac{M}{M+m}\right) \frac{V_{pp}^3}{m^2} \quad (2\text{-}14)$$

Here, n_n is the collision gas number density, σ is the collision cross section of the ion, K_v is the proportionality constant relating v (the ion velocity) to v_{max} (the maximum velocity of the activated ion), f_E is an assumed constant fraction of the maximum energy in the center-of-mass reference frame during SORI that is deposited into the parent ion per collision, t_{coll} is the time during which collisions take place (the SORI excitation event length), β is the trapping cell geometry factor, q is the charge on the parent ion, d is the diameter of the trapping cell, Δf is the frequency offset of the excitation pulse from the resonant frequency of the parent ion, m is the mass of the parent ion, M is the mass of the neutral collision gas, and V_{PP} is the peak-to-peak amplitude of the SORI excitation pulse.

A frequency offset of 1-2 kHz is believed to be the most favorable in order to minimize isotopic distortion and width of the blind spot i.e. a frequency range where ion excitation leads to ejection of the ions.[23] In our experiments, the frequency offset is arbitrarily chosen to be 1 kHz off resonance and the rest of the terms in Equation 2-14 are constant except σ, M, m and V_{PP}. As a consequence, E_{SORI} is proportional to the experimental parameters represented by Equation 2-15:

$$E_{SORI} \propto \sigma \left(\frac{M}{M+m}\right) \frac{V_{pp}^3}{m^2} \quad (2\text{-}15)$$

The collision cross section is assumed to be independent of ion velocity and in the hard sphere collision regime. It can be computed by measuring the solvent accessible surface area of the ion or by experiment, either using the ion mobility technique[24] or by utilizing CRAFTI.[5]

2.3.2 Cross sectional Areas by FTICR-MS (CRAFTI)

One of the newest methods to detect collision cross sections, referred to as CRAFTI, involves using FTICR. FTICR is typically operated at lower pressures than ICR to prevent collisional broadening. Several models for ion motion in FTICR have been proposed,[25] which are based on ion-neutral collisions using a frictional damping term in the equation of ion motion. The Langevin model[26] assumes the ion is a point charge and the neutral has an ion-induced dipole. In this model the ion-neutral collision cross section is inversely related to the ion velocity and the ion–neutral collision frequency is independent of it. This model results in a linear equation for ion motion in both time and frequency domain and predicts an exponentially damped ICR signal having a Lorentzian-shaped frequency spectrum. It provides a good approximation for low mass ion collisions with low mass neutrals but fails for higher mass ions where the hard-sphere model is more rational. The hard–sphere model,[16] which assumes elastic collision between ion and neutral, provides that the collision frequency depends on ion velocity, while the collision cross section is independent of it. A nonlinear equation of motion is obtained that can be solved numerically to give an FTICR line shape characterized by a narrow center and broad wings.

Accurate description of detection in FTICR may not be provided by the frictional damping model, as the signal decay is predominantly due to dephasing of ion packets by collisions with the neutral gas. A kinetic approach to model the FTICR signal is described by Yang et al.[5] in which a few assumptions are made. First, it is assumed that the FTICR signal depends on the number of coherently orbiting ions. The second assumption is that when an ion undergoes a collision, it is scattered out of the coherent packet leading to signal decay. The line shape broadens as pressure is varied. This eliminates any contribution to line broadening except by collisions (Figure 2.7).

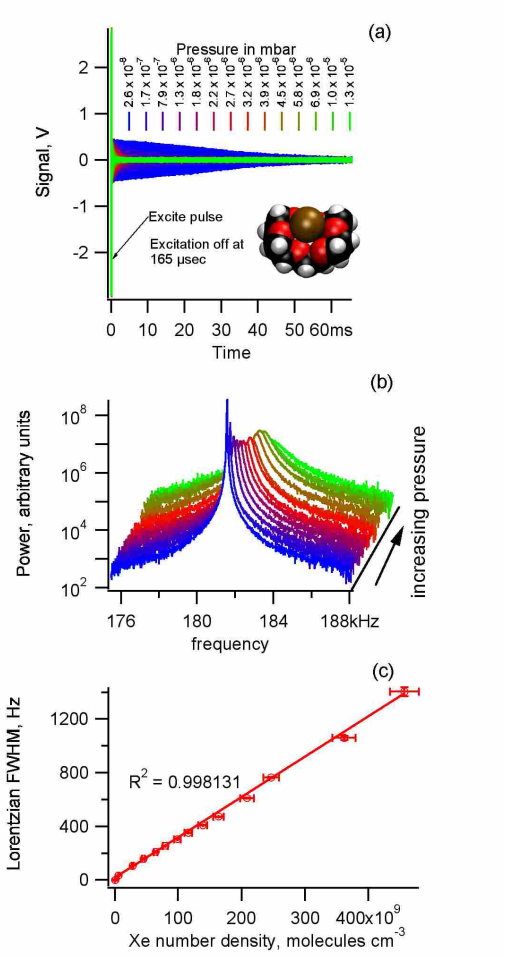

Figure 2.7 Change in FTICR linewidth for 18-crown-6•Cs^+ complex (inset) vs background Xe (a) Time domain signals over a range of Xe pressures (b) Power mode frequency domain spectra corresponding to the time domain transients of (a).(c) Full width at half maximum (FWHM) linewidths as a function of Xe number density, showing excellent linearity.(Reprinted WITH PERMISSION from "Collision cross sectional areas from analysis of fourier transform ion cyclotron resonance line width: a new method for characterizing molecular structure" by Yang et al., 2012, Anal. Chem., 4851–4857, copyright (2012) American Chemical Society)

The cross section is calculated by:

$$\sigma = \frac{FWHM}{n_n}\frac{(m+M)}{M}\frac{m}{q}\frac{d}{\beta V_{PP} t_{exc}} \tag{2-16}$$

Here $\frac{FWHM}{n_n}$ is the slope of the line in the plot of power spectrum FWHM linewidth vs. neutral number density, n_n. β is the cell geometry factor (0.897 for the Bruker Infinity cell used here), *Vpp* is the peak-to-peak RF excitation amplitude, t_{exc} is the duration of the RF excitation, *d* is the trapping cell diameter, *m* is the mass of the ion and *M* is the mass of the neutral.

Yang et. al.[27] demonstrated the most important factors affecting the CRAFTI cross section to be ion kinetic energy (Figure 2.8a) and the nature of the collision gas (Figure 2.8b). The cross sections are found to increase as the corresponding kinetic energy is increased, until a limiting value at a high energy is reached while operating in the center of mass reference frame. These results have been found to be consistent with all the collision gases in which CRAFTI has been performed. The limiting value of cross section reached at high energy was found to be dependent on the internal degrees of freedom of the ion. On the other hand, the cross sections are found to decrease with increasing mass of the collision gas. This can be attributed to the reduced mass term in the cross section calculation in Equation 2-16, which in turn increases with mass of the neutral collision gas. In addition to the mass effect, the physical size of the collision gas also has an important effect. For example, SF_6 (146 Da) is found to give higher cross section than Xe (132 Da). The analytical sensitivity is found to be greater for lighter gases as long as the collision gas is massive enough to dephase the ion in a single collision. A monoatomic light gas like Ar can be argued to represent the best compromise, keeping in consideration the need to achieve the maximum center of mass kinetic energy achievable with the lightest possible collision gas.

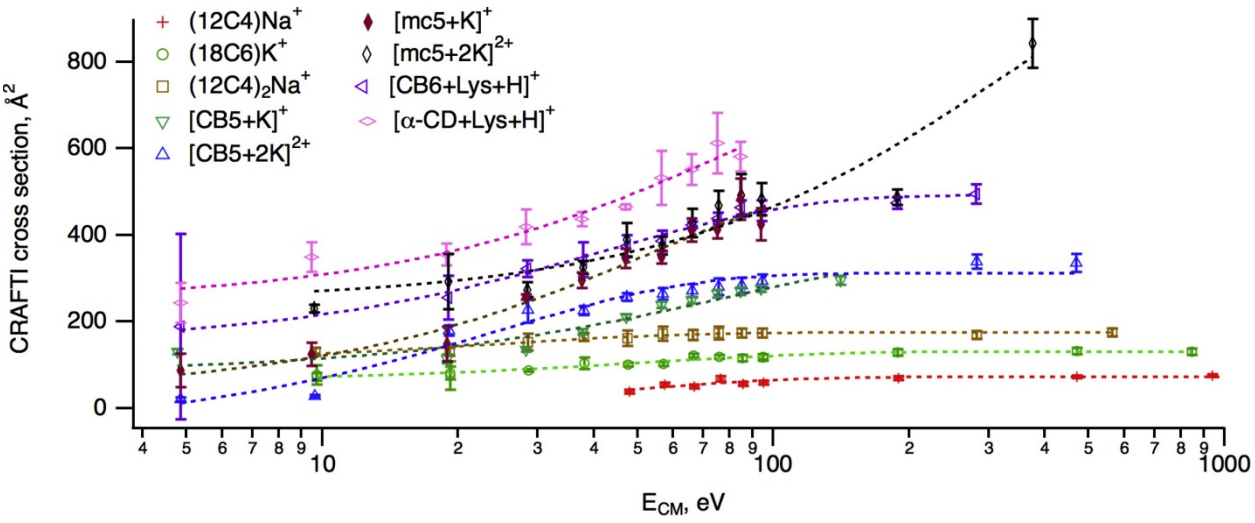

(a)

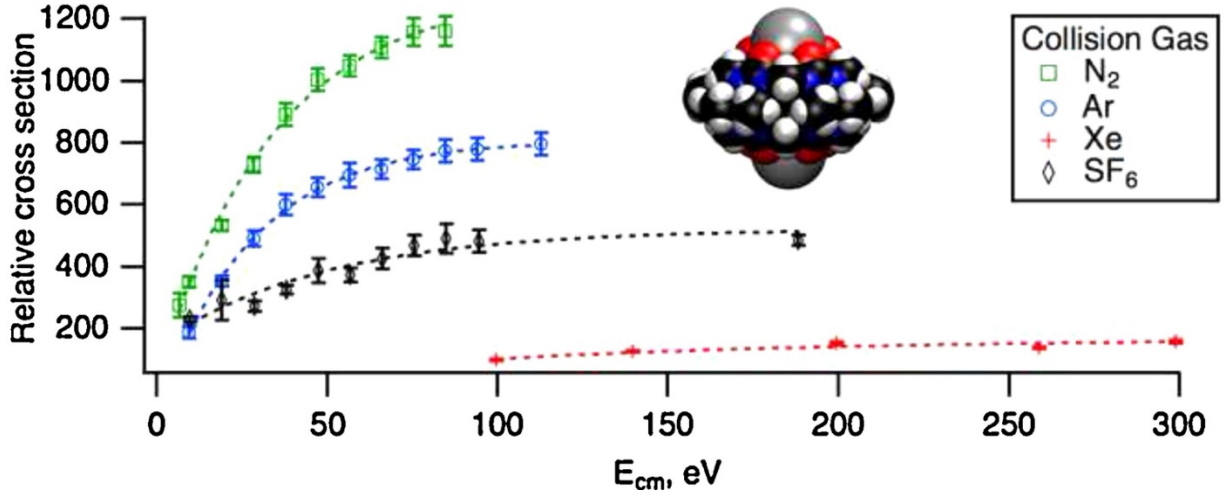

(b)

Figure 2.8 Dependence of CRAFTI cross sections on (a) kinetic energy (determined using SF_6 collision gas) (b) Collison gas *(Reprinted with permission from "Effects of kinetic energy and collision gas on measurement of cross sections by Fourier transform ion cyclotron resonance mass spectrometry" by Yang et al., 2015, Int. J. Mass spectrom., 143–150, copyright (2014) Elsevier B.V.)*

In order to determine accurate and precise CRAFTI cross sections, the collision gas pressure in the trapping cell must be measured accurately. Earlier the pressure for CRAFTI experiments was measured using a cold cathode ionization gauge (model IKR050, Balzers) which is seated about 1 m from the trapping cell, out of the high field region of the instrument. Depending on the type of collision gas used, the pressures were adjusted based on the relative sensitivity of the cold cathode gauge using the method of Bartmess and Georgiadis.[28] Their method assumes that the gauge is calibrated for nitrogen and the reading is adjusted for the relative ease of ionizing the gas by multiplying the indicated pressure with the sensitivity factor for the gas used. The cold cathode gauge works on the principle of ionization of gas molecules, which causes the positive ions to move towards the negative electrode, resulting in a current directly proportional to the pressure.[29] Considering the gauge is outside the trapping cell, the measured pressure must be adjusted to reflect the true pressure in the cell. Jones and Dearden addressed this problem using a new method to measure pressure inside the FTICR trapping cell.[7] They determined absolute pressures by measuring Ar^+ linewidths in Ar background gas. The typical experiment for pressure measurement begins with pulsing of neutral argon gas and ionization from an electron gun to create Ar^+ ions. Thereafter neutral argon is again leaked into the trapping cell for different pressurization durations and the resulting linewidth of Ar^+ in neutral Ar is measured. A collection of Ar^+ in Ar kinetic-energy resolved momentum transfer cross sections is available from the literature[30] and can be used to convert the measured linewidths into absolute pressures using Equation 2-17:

$$n_n = \frac{FWHM}{\sigma}\frac{(m+M)}{M}\frac{m}{q}\frac{d}{\beta V_{PP} t_{exc}} \tag{2-17}$$

The terms are the same as explained earlier for Equation 2-16 and only the pressure and cross section have changed places.

Pressures measured in this way are calibrated for Ar and are not subject to uncertainty from chemical sensitivity. They are measured in the trapping cell so they are not subject to errors resulting from measurement at a point remote from the trapping cell. They do not involve ion current measurements, so they are not adversely affected by the magnetic field. These pressure measurements were performed twice (before and after) for cross section measurements. The average pressure was used in determining the CRAFTI cross section for molecular complexes. In 2015, collision cross section measurement using FTICR was performed on biomolecules like ubiquitin and cytochrome c using the similar principle, but with a time-domain data processing method to simultaneously extract both ion *m/z* and CCS from the image current.[31]

The ensuing determination of cross section and conformation can be applied in several scientific domains. One of the most important potential uses is drug discovery, where cross section information can be used to screen potential drugs for disease management. Structure-activity relationships can be established by exclusion of those complexes that are too big, too small, too rigid or too flexible in ligand binding. An example is organoruthenium complexes, which form adducts with DNA oligonucleotides that have been analyzed as potential anticancer agents.[32] Structural characterization of small peptides is another application. Human insulin oligomers have also been characterized using cross section measurements, which can be used to examine constitutional effects caused by changes in protein sequence.[33] Other important applications include structural information for bigger molecular aggregates like polypeptides, proteins, and nucleotides, which can provide insights into the foundations of protein folding, critical to the development of protein formulations and gene therapy.

2.4 References

1. Marshall, A. G.; Hendrickson, C. L.; Jackson, G. S., Fourier transform ion cyclotron resonance mass spectrometry: a primer. *Mass Spectrom. Rev.* 1998, *17* (1), 1-35.

2. Noest, A.; Kort, C., Aspects of FT-ICR software—III: Chirp Excitation. *Comput. Chem.* 1983, *7* (2), 81-86.

3. Guan, S.; Marshall, A. G., Stored waveform inverse Fourier transform (SWIFT) ion excitation in trapped-ion mass spectometry: Theory and applications. *Int. J. Mass Spectrom. Ion Phys.* 1996, *157*, 5-37.

4. Schmidt, E. G.; Arkin, C. R.; Fiorentino, M. A.; Laude, D., Application of simultaneous excitation/detection to generate real-time excitation profiles in fourier transform ion cyclotron resonance mass spectrometry. *J. Am. Soc. Mass Spectrom.* 2000, *11* (11), 1009-1015.

5. Yang, F.; Voelkel, J. E.; Dearden, D. V., Collision cross sectional areas from analysis of fourier transform ion cyclotron resonance line width: a new method for characterizing molecular structure. *Anal. Chem.* 2012, *84* (11), 4851-4857.

6. Dempster, A., A new method of positive ray analysis. *Phy. Rev.* 1918, *11* (4), 316.

7. Jones, C. A.; Dearden, D. V., Linewidth Pressure Measurement: A New Technique for High Vacuum Characterization. *J. Am. Soc. Mass Spectrom.* 2015, *26* (2), 323-329.

8. Yamashita, M.; Fenn, J. B., Electrospray ion source. Another variation on the free-jet theme. *J. Phys. Chem.* 1984, *88* (20), 4451-4459.

9. Taylor, G. In *Disintegration of water drops in an electric field*, Proceedings of the Royal Society of London A: Mathematical, Physical and Engineering Sciences, The Royal Society: 1964; pp 383-397.

10. Cech, N. B.; Enke, C. G., Practical implications of some recent studies in electrospray ionization fundamentals. *Mass Spectrom. Rev.* 2001, *20* (6), 362-387.

11. Marshall, A. G.; Hendrickson, C. L., Fourier transform ion cyclotron resonance detection: principles and experimental configurations. *Int. J. Mass spectrom.* 2002, *215* (1), 59-75.

12. Hendrickson, C. L.; Quinn, J. P.; Kaiser, N. K.; Smith, D. F.; Blakney, G. T.; Chen, T.; Marshall, A. G.; Weisbrod, C. R.; Beu, S. C., 21 Tesla Fourier Transform Ion Cyclotron Resonance Mass Spectrometer: A National Resource for Ultrahigh Resolution Mass Analysis. *J. Am. Soc. Mass Spectrom.* 2015, *26* (9), 1626-1632.

13. Marshall, A. G., Milestones in Fourier transform ion cyclotron resonance mass spectrometry technique development. *Int. J. Mass spectrom.* 2000, *200* (1), 331-356.

14. Florida Inventors Hall of Fame Announces 2016 Inductees. 2016.

15. (a) Bogdanov, B.; Smith, R. D., Proteomics by FTICR mass spectrometry: top down and bottom up. *Mass Spectrom. Rev.* 2005, *24* (2), 168-200; (b) Brown, S. C.; Kruppa, G.; Dasseux, J. L., Metabolomics applications of FT-ICR mass spectrometry. *Mass Spectrom. Rev.* 2005, *24* (2), 223-231; (c) Dearden, D. V.; Liang, Y.; Nicoll, J. B.; Kellersberger, K. A., Study of gas-phase molecular recognition using Fourier transform ion cyclotron resonance mass spectrometry (FTICR/MS). *J. Mass Spectrom.* 2001, *36* (9), 989-997; (d) Feng, X.; Siegel, M. M., FTICR-MS

applications for the structure determination of natural products. *Anal. Bioanal. Chem.* 2007, *389* (5), 1341-1363.

16. Laskin, J.; Futrell, J. H., Activation of large lons in FT-ICR mass spectrometry. *Mass Spectrom. Rev.* 2005, *24* (2), 135-167.

17. Gauthier, J.; Trautman, T.; Jacobson, D., Sustained off-resonance irradiation for collision-activated dissociation involving Fourier transform mass spectrometry. Collision-activated dissociation technique that emulates infrared multiphoton dissociation. *Anal. Chim. Acta* 1991, *246* (1), 211-225.

18. Tolic, L. P.; Bruce, J. E.; Lei, Q. P.; Anderson, G. A.; Smith, R. D., In-trap cleanup of proteins from electrospray ionization using soft sustained off-resonance irradiation with Fourier transform ion cyclotron resonance mass spectrometry. *Anal. Chem.* 1998, *70* (2), 405-408.

19. Kelleher, N. L.; Lin, H. Y.; Valaskovic, G. A.; Aaserud, D. J.; Fridriksson, E. K.; McLafferty, F. W., Top down versus bottom up protein characterization by tandem high-resolution mass spectrometry. *J. Am. Chem. Soc.* 1999, *121* (4), 806-812.

20. Flora, J. W.; Hannis, J. C.; Muddiman, D. C., High-mass accuracy of product ions produced by SORI-CID using a dual electrospray ionization source coupled with FTICR mass spectrometry. *Anal. Chem.* 2001, *73* (6), 1247-1251.

21. Yang, F.; Dearden, D. V., Guanidinium-capped cucurbit [7] uril molecular cages in the gas phase. *Supramol. Chem.* 2011, *23* (01-02), 53-58.

22. Zhang, H.; Ferrell, T. A.; Asplund, M. C.; Dearden, D. V., Molecular beads on a charged molecular string: α, ω-alkyldiammonium complexes of cucurbit [6] uril in the gas phase. *Int. J. Mass spectrom.* 2007, *265* (2), 187-196.

23. Mortensen, D. N.; Jones, C. A.; Dearden, D. V., Appropriate choice of event length in sustained off-resonance irradiation collision-induced dissociation (SORI-CID) experiments: Activated ion collision-induced dissociation. *Int. J. Mass spectrom.* 2012, *330*, 241-245.

24. Clemmer, D. E.; Jarrold, M. F., Ion mobility measurements and their applications to clusters and biomolecules. *J. Mass Spectrom.* 1997, *32* (6), 577-592.

25. Guan, S.; Li, G.-Z.; Marshall, A. G., Effect of ion-neutral collision mechanism on the trapped-ion equation of motion: a new mass spectral line shape for high-mass trapped ions. *Int. J. Mass Spectrom. Ion Phys.* 1997, *167*, 185-193.

26. Marshall, A. G.; Comisarow, M. B.; Parisod, G., Relaxation and spectral line shape in Fourier transform ion resonance spectroscopy. *J. of Chem. Phys.* 1979, *71*, 4434.

27. Yang, F.; Jones, C. A.; Dearden, D. V., Effects of kinetic energy and collision gas on measurement of cross sections by Fourier transform ion cyclotron resonance mass spectrometry. *Int. J. Mass spectrom.* 2015, *378*, 143-150.

28. Bartmess, J. E.; Georgiadis, R. M., Empirical methods for determination of ionization gauge relative sensitivities for different gases. *Vacuum* 1983, *33* (3), 149-153.

29. Peacock, R.; Peacock, N.; Hauschulz, D., Comparison of hot cathode and cold cathode ionization gauges. *J. Vac. Sci. Technol., A* 1991, *9* (3), 1977-1985.

30. Phelps, A. V., Cross Sections and Swarm Coefficients for Nitrogen Ions and Neutrals in N_2 and Argon Ions and Neutrals in Ar for Energies from 0.1 eV to 10 keV. *J. Phys. Chem. Ref. Data* 1991, *20* (3), 557-573.

31. Guo, D.; Xin, Y.; Li, D.; Xu, W., Collision cross section measurements for biomolecules within a high-resolution FT-ICR cell: theory. *Phys. Chem. Chem. Phys.* 2015, *17* (14), 9060-9067.

32. Williams, J. P.; Lough, J. A.; Campuzano, I.; Richardson, K.; Sadler, P. J., Use of ion mobility mass spectrometry and a collision cross-section algorithm to study an organometallic ruthenium anticancer complex and its adducts with a DNA oligonucleotide. *Rapid Commun. Mass Spectrom.* 2009, *23* (22), 3563-3569.

33. Salbo, R.; Bush, M. F.; Naver, H.; Campuzano, I.; Robinson, C. V.; Pettersson, I.; Jørgensen, T. J.; Haselmann, K. F., Traveling-wave ion mobility mass spectrometry of protein complexes: accurate calibrated collision cross-sections of human insulin oligomers. *Rapid Commun. Mass Spectrom.* 2012, *26* (10), 1181-1193.

Chapter 3 Conformational Analysis of n-Alkylamine Complexes with Crown Ethers Using FTICR "CRAFTI" Technique

3.1 Abstract

We report relative dephasing cross sections for non-covalent complexes formed between cyclic polyethers (e.g. 12-crown-4 (12C4), 15-crown-5 (15C5) and 18-crown-6 (18C6) and different alkyl ammonium ions using Fourier transform ion cyclotron resonance ("CRAFTI") techniques at 130 eV in the center-of-mass reference frame. The collision cross section (CCS) values were found to correlate with the size and mass of the polyether and ammonium ion. The experimental determinations were further corroborated with *in silico* Boltzmann-weighted computational cross sections for the same ions computed from structures determined using molecular mechanics. The CRAFTI measurements correlated well with the results from momentum transfer cross sections as well as drift ion mobility (IMS) indicating that CRAFTI provides accurate structural information. However, the absolute CCS values differed significantly between IMS and CRAFTI. This could be attributed to errors in measurements in either the collision gas pressure or excitation voltage. Complexes of polyethers with normal and tertiary-alkyl amines gave different CCS, which is attributed to small conformational differences for these ions and further shows the sensitivity of CRAFTI in determining subtle differences. This study demonstrates the IMS-like broad versatility of the CRAFTI method.

3.2 Introduction

Accurate determination of structure and conformation of a molecule is critical to understanding and eventually optimizing its performance. Many examples can be found in the biopharmaceutical industry where the conformation of a candidate drug at a biological receptor

site determines its activity and therefore its therapeutic potential.[1] For many molecules, minor conformational changes in the molecule can have profound effects on its activity.[2] While several molecular conformation descriptors exist, collision cross section (CCS), conveying information about the shape and size of the molecule, is arguably the most popular.[3]

A particularly popular method is a hybrid of ion mobility (IM) coupled with mass spectrometry (IM-MS) that has been widely used to investigate a wide range of molecules ranging from small to large macro/bio molecules.[4] Despite its popularity, IM-MS suffers certain limitations, the most critical one being conformational distortion by multiple collisions with the buffer gas and ion heating as the molecule moves through a drift tube.[5] Furthermore, instrument calibration is needed before every measurement as the observed CCS is a strong function of the temperature and pressure.[6] These drawbacks when coupled with increasing demands for CCS determination have directed research towards novel method development.

One such method is the MS based CRAFTI (cross sectional areas by Fourier transform ion cyclotron resonance) technique, which was first introduced by our group.[7] This technique is based on dephasing of the ion signal in FTICR by single collisions under controlled pressure of the neutral background gas. The broadening of the mass spectral line width and hence the corresponding signal decay rate relates directly to the collision cross section of ion. In contrast, IM-MS involves multiple thermal collisions between ions and the carrier gas (typically He or N_2).The fundamental difference between the two methods make absolute agreement in the measured value rather poor, however the relative trends between the two methods are generally well correlated.[7a] Recently, peptides were investigated using a method very similar to CRAFTI, the difference being primarily in the data analysis technique.[8] This demonstrates the IM-MS-like broad versatility of the CRAFTI method in sampling chemical space.

However, a particular complication arises when polyatomic ions are analysed using CRAFTI. Dephasing of such ions is not restricted to the momentum transfer collisions described previously, but ion dissociation can also play a critical part. Above a certain threshold collision energy, which may be lower than the energy needed to scatter away the ion, it is possible to induce ion dissociation. Such dissociation would change the cyclotron frequency, dampen the time domain signal, and broaden the frequency domain linewidth, as the ions are no longer a part of the coherent ion packet. Thus, caution must be exercised when analysing CRAFTI results because of the added broadening attributed to dissociation.[9]

With this background, the current article investigates simple crown ether inclusion complexes with alkyl monoamines which are expected to have similar binding energies and hence similar dissociation behaviour.[10] Crown ether complexes have been extensively studied as model systems for biological host-guest interactions.[11] The current article reports relative dephasing cross sections for crown ether–alkyl monoamine complexes measured using CRAFTI, which are compared against published IM-MS values[12] and computational molecular modelling-based determinations to lend further structural insight about polyether complexes.

3.3 Experimental

3.3.1 Materials

The crown ethers (Figure 3.1) used in this study were 12-crown-4 (C4), 15-crown-5 (C5), and 18-crown-6 (C6), and the aminoalkanes used were n-alkyl monoamine (x = 0-9, where x is the number of carbon atoms in the alkyl chain). All the chemicals were purchased from Sigma-Aldrich (St. Louis, MO) and used as supplied. Electrospray solutions were prepared at a concentration of 100 μM in crown ether and 200 μM in amine dissolved in 50/50 methanol/water with 1% acetic acid. Argon gas was purchased from Airgas (Radnor, PA) at a nominal purity of 99.995%.

3.3.2 Instrumentation

All experiments were carried out using a Bruker model APEX 47e Fourier transform ion cyclotron resonance mass spectrometer (FTICR-MS) with an Infinity trapping cell[13] and a micro-electrospray source modified from an Analytica (Branford, MA) design, equipped with a heated metal capillary drying tube based on the design of Eyler.[14] Radio frequency (rf) excitation amplitudes were measured using an oscilloscope at the output of the final excitation amplifier. The instrument was controlled using a MIDAS Predator data system (National High Magnetic Field Laboratory; Tallahassee, FL).[15] Argon was introduced as collision gas using a Freiser-type pulsed leak valve.[16] It consists of a 0.004" orifice pressurization solenoid valve backed by a 28 psig Ar supply line and a 0.039" orifice evacuation solenoid valve connected to a mechanical vacuum pump (both valves from General Valve Corp.; Fairfield, NJ). Both solenoid valves were connected to the high-pressure side of a precision variable leak valve (Varian; Palo Alto, CA). Steady-state pressures obtained with the pulsed leak system were varied by varying the length of time the pressurization solenoid valve was left open. A tool command language (TCL) script was used to automatically modulate the pressure during excitation by varying the duration of the pulsed leak events.

3.3.3 Procedures

Absolute pressures were measured by measuring Ar+ linewidths in Ar background gas as described in detail elsewhere.[17] These pressure measurements were performed both before and after each crown ether-monoamine CCS measurement and the average pressure was used in determining the CRAFTI cross sections, although no major pressure drifts were seen.

The procedure for the CCS measurements is described in detail elsewhere.[7a] Typically, CRAFTI-based CCS are measured by pulsing Ar into the FTICR trapping cell to a constant

pressure using the pulsed leak valve, then exciting the ions at their resonant cyclotron frequency with an amplitude and duration appropriate to achieve the desired kinetic energy (in this case, a center-of-mass frame energy of 130 eV, a value arbitrarily chosen because it allowed collection of strong signal for all of the target ions with a short excitation event). The resulting time domain image current signal yields a frequency domain power spectrum after Fourier transformation. A set of power spectral full width at half maximum (FWHM) linewidths measured at various Ar pressures is collected. Plots of linewidths vs. collision gas number density are generally linear, and the slope is used to determine the CRAFTI CCS. The CRAFTI experimental results were processed using the Igor Pro software package (version 6.34a, Wavemetrics, Lake Oswego, OR). Details for the analysis process are reported elsewhere.[7a]

3.3.4 Computational cross section

Molecular structures were obtained using the Spartan '08 package (Wavefunction, Inc.; Irvine, CA) for conformational searching using the MMFF force field provided in the package, requesting 10,000 starting conformers (but systematic searches sometimes completed after examining fewer than 10,000 structures). For each protonated crown ether-monoamine complex, the atomic coordinates for the five conformers with the lowest MMFF energies were put into the MOBCAL[18] program for calculation of low energy momentum transfer cross sections in helium. The modeling was performed using the same recipe as described previously.[7a]

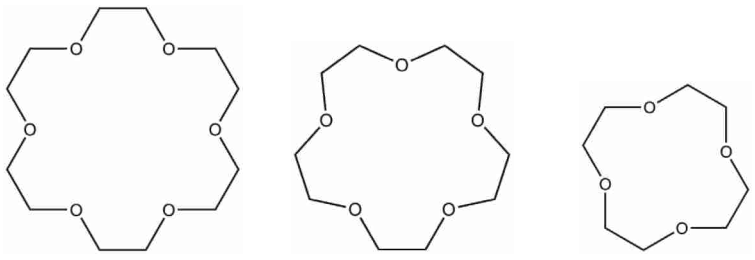

Figure 3.1. Structures of the cyclic polyethers used in this study

3.4 Results and discussion

3.4.1 Experimental CRAFTI cross sections for crown ether-n-alkyl monoamine complex

3.4.1.1 Variation in CCS as a function of crown ether ring size and alkyl monoamine chain length

Host-guest complexes between crown ethers and protonated amines are formed readily in the gas phase giving 1:1 singly-charged complexes. These prototype amine-ether complexes have been extensively studied in supramolecular chemistry and can be used for validating the CRAFTI method. As the values of CRAFTI cross sections are strongly dependent on the kinetic energy in the center-of-mass frame, the measurements were performed for each ion at a constant center-of-mass kinetic energy. Cross sections for protonated crown ether- alkylmonoammonium complexes, measured using CRAFTI at a kinetic energy of 130 eV in the center-of-mass frame, are listed in Table 3.1. A few trends are clearly evident from the tabulated values. The first observation is that for all the crown ether-alkyl monoamine complexes, CCS increases monotonically with alkylammonium chain length. For guest ions of the same chain length, the cross sections were found to increase in the order of the size of the crown ether ring: 12-crown-4 < 15-crown-5 < 18-crown-6. Figure 3.2 shows a plot of CRAFTI cross section vs. the number of carbon atoms in the alkylamine chains. The slope of this plot gives the cross sectional area of the methylene group (-CH_2-) in the gas phase and in all the crowns it was found to be 48.3 ± 2.4 $Å^2$ at 130 eV. To our knowledge, this is the first report of the cross section per methylene group in the gas phase.

An interesting feature of the polyether-amine complexes is their hydrogen bonding dictated gas phase stability, with the primary hydrogen bonding interactions between the amine donors and the oxygen receptor sites. Increasing the crown cavity size (Table 3.2), and the number of oxygen atoms of the host ether increases the affinity for the protonated amine. The corresponding affinity of the guest ammonium ion increases with increase in size/chain length of the substituent due to

additional inductive stabilization of the side chain by van der Waals interaction. As these complexes are expected to have similar binding energies and dissociation behaviour, we expected the collision cross sections to be dependent primarily on their corresponding sizes. The linear correlation of the CCS with increasing size/chain length of substituent (Figure 3.2) confirms this hypothesis.

Table 3.1 Cross sections (Å^2) for protonated crown ether-alkyl monoamine complexes using CRAFTI.

n in $[H(CH_2)_nNH_2]$	CRAFTI Collision cross section (Å^2)		
	12-crown-4	15-crown-5	18-crown-6
0	284.4 ± 2.1	379.9 ± 3.1	506.0 ± 2.9
1	311.4 ± 3.1	410.4 ± 2.4	534.6 ± 3.1
2	342.0 ± 4.1	440.2 ± 3.4	575.9 ± 3.0
3	385.5 ± 4.0	479.9 ± 3.7	614.6 ± 2.5
4	431.2 ± 4.6	557.6 ± 2.9	681.6 ± 6.0
5	468.9 ± 5.0	586.1 ± 4.8	707.9 ± 5.0
6	526.9 ± 7.2	647.9 ± 6.6	775.5 ± 3.0
7	580.5 ± 6.4	698.4 ± 5.7	840.8 ± 3.8
8	631.3 ± 6.2	763.2 ± 9.1	878.5 ± 7.2
9	683.1 ± 7.4	809.7 ± 8.7	945.7 ± 8.0

Table 3.2 Relative cavity sizes of crown ethers[19]

Polyether ring	Cavity Size, Å
12-Crown-4	1.2-1.5
15-Crown-5	1.7-2.2
18-Crown-6	2.6-3.2

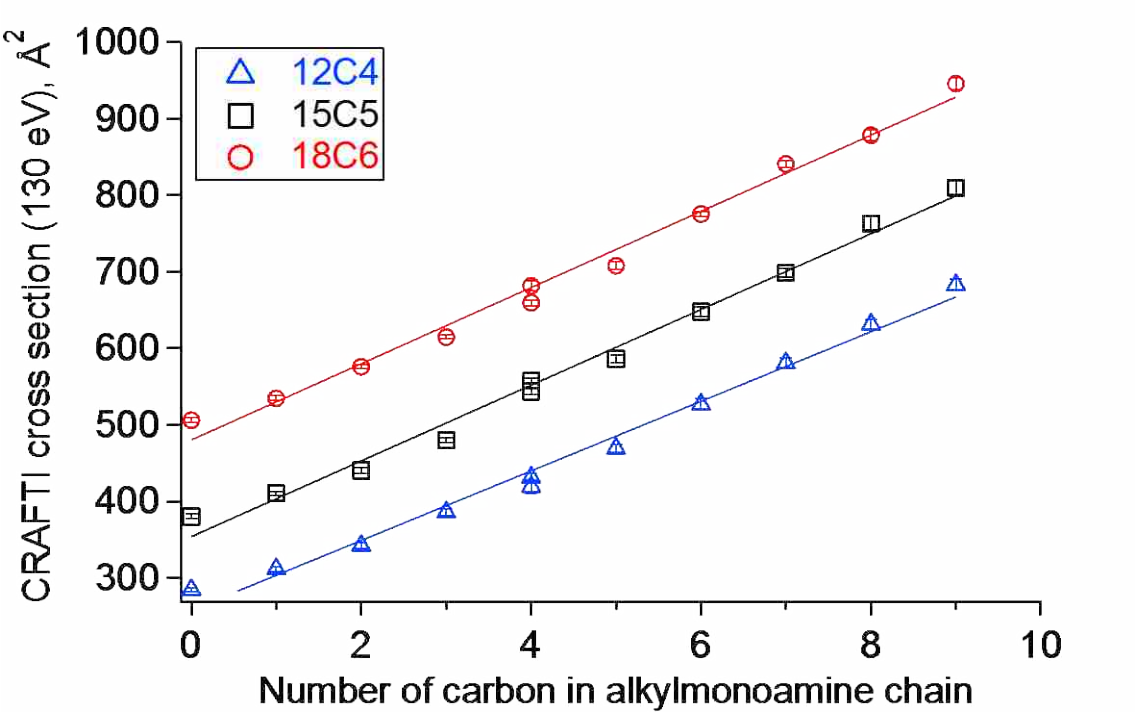

Figure 3.2 Cross sections ($Å^2$) for protonated crown ether-alkyl monoamine complexes using CRAFTI.

3.4.1.2 CCS measurements of isomeric amines complexed with crown ethers

The CRAFTI measurements were undertaken for complexes between crown ether host molecules and isomers of butylamine as guests to determine whether CCS for different isomers can be detected and quantified. The two guest molecules studied were *n*-butylamine and *t*-butylamine. Each butylamine isomer-crown ether sample was injected separately and their collision cross sections were measured using CRAFTI and compared.

Table 3.3 Cross sections ($Å^2$) of n- and t-butylamine with C4, C5 and C6.

	CRAFTI Collision cross sections, ($Å^2$)		
Host/Guest	*n*-butylamine	*t*-butylamine	Rel. Difference (%)
12-Crown-4	431.2 ± 4.6	419.1 ± 8.7	2.8
15-Crown-5	557.6 ± 2.9	543.3 ± 3.6	2.6
18-Crown-6	681.6 ± 6.0	659.6 ± 3.9	3.2

Table 3.3 indicates that the *n*–butyl isomer has a greater cross section than its *t*-butyl counterpart for each complex with the three crown ethers. This result is expected, given the linear structure of the *n*-butyl analog in comparison to the branched chain in *t*-butyl, which makes the latter more compact. Unfortunately, experimental elucidation of CCS differences for isomeric species is cumbersome owing to insufficient resolving power from all the currently practiced techniques (CRAFTI, IMS, and TWIMS).

3.4.2 Comparison with IMS results

Ion-mobility spectrometry–mass spectrometry (IMS-MS) is currently considered the gold standard for gas phase collision cross section measurements. IMS measures momentum transfer collisions. An ionized sample is introduced into a drift tube filled with buffer gas and gaseous ions are accelerated under the influence of a weak electric field. Low energy collisions occur between the ion and the buffer gas (low vacuum or atmospheric pressure conditions). Ions with higher cross section suffer more collisions; consequently, they have a longer drift time across the tube. The collision cross section is measured in IMS-MS using Equation 3-1 below.

$$\Omega = \frac{3ze}{16N_0}\left(\frac{2\pi}{\mu kT}\right)^{1/2}\frac{1}{K_0} \tag{3-1}$$

Here Ω is the collision cross-section of the ions, ze is the charge of the ion, k is Boltzmann's constant, T is the temperature, μ is the reduced mass of the collision system, N_0 is the number density of an ideal gas at STP, and K_0 is the reduced mobility for the ion. Ions that are more compact will have a higher mobility through the drift tube and therefore a smaller cross section than larger ions. For the purposes of validation, it is important to establish correlation between the newer CRAFTI technique and the gold standard IMS method.

Table 3.4 Cross sections ($Å^2$) of protonated crown ether-alkyl monoamine complexes using Drift Ion mobility

n in $[H(CH_2)_nNH_2]$	CRAFTI Collision cross section ($Å^2$)		
	12-crown-4	15-crown-5	18-crown-6
0	109.5	118.9	132.3
3	121.7	128.9	142.2
4	126.1	135.5	146.1

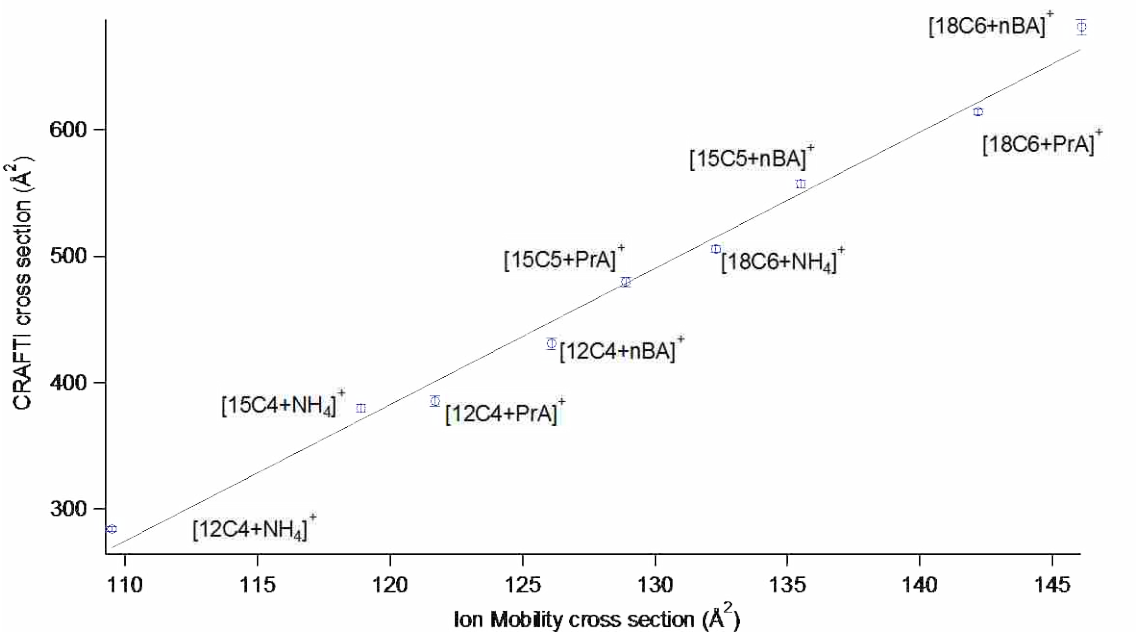

Figure 3.3 Correlation between CRAFTI cross section in argon and cross section from drift ion mobility[24]

Figure 3.3 highlights the strong linear correlation between the IMS and CRAFTI methods ($R^2 = 0.9892$). Despite the linear correlation, absolute CCS values measured using CRAFTI and IMS differ significantly. The CRAFTI measurements span a much wider range of values. The CRAFTI values have not been calibrated to match the IMS values, but the linear correlation shows that it could be easily done.

3.4.3 Comparison of CRAFTI cross section with cross sections computed using the exact hard sphere scattering method

One of the most important practical applications of CCS measurements is to confirm structures generated in silico from molecular modelling. Ideally, the convergence of the computationally predicted and the experimentally determined values would unequivocally confirm the structure. One of the highlights of traditional IMS measurements is their correlation with molecular structure, which lends great credibility and analytical value. With this in mind, CRAFTI measurements were also compared against experimental values. The correlation of the experimental data sets with Boltzmann weighted average exact hard sphere scattering (EHSS) based CCS is shown in Figure 3.4.

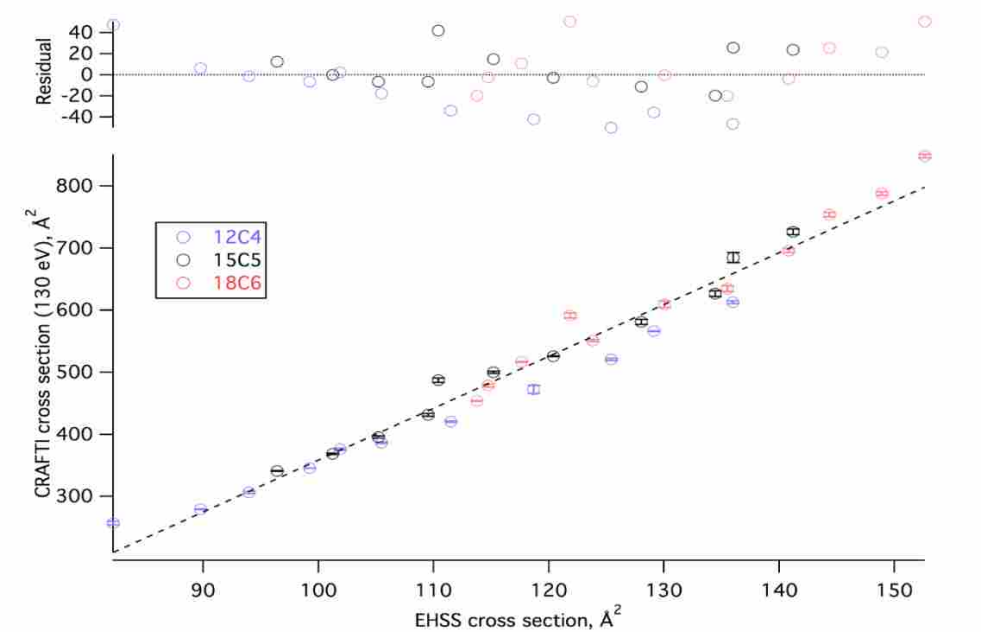

Figure 3.4 Correlation of experimental CCS measurements with Boltzmann-weighted CCS computed using the exact hard sphere (EHSS) scattering method from molecular models

The computational values represent those generated from the EHSS method (Table 3.5). As with the IMS measurements, Boltzmann weighted average EHSS-based computed CCS values were found to be linearly correlated (R^2 = 0.9748) with CRAFTI measurements. There is no systematic difference between the experimental and computational values for different complexes, which is demonstrated by the random error distribution in the residual plot (Figure 3.4). The CRAFTI based CCS were significantly higher than the computed values. In contrast, the absolute agreement between computed and experimentally determined values is expected to be better for IMS. This can be attributed to the similarity in the computational EHSS and experimental IMS methods, both of which are based on momentum transfer cross sections due to multiple low energy collisions. The MOBCAL program used to compute the EHSS cross sections is designed to model IMS measurements, so the good absolute agreement is expected. In contrast, CRAFTI involves single high-energy collisions with Ar neutrals. Ideally, the CRAFTI measurements should also be

compared against a computational procedure that models such collisions. This highlights the robustness of the methods employed and their sensitivity to the actual measurement conditions. Given the linear correlation with the computed values, they could easily be used for calibration of CRAFTI based measurements to produce measurements equivalent to those of IMS, a practice that is routine for travelling-wave ion mobility spectrometry (TWIMS).

Table 3.5 Cross sections ($Å^2$) of protonated crown ether-alkyl monoamine complexes using EHSS.

n in $[H(CH_2)_nNH_2]$	CRAFTI Collision cross section ($Å^2$)		
	12-crown-4	15-crown-5	18-crown-6
0	82.2	96.4	113.8
1	89.7	101.2	114.7
2	94.0	105.2	117.6
3	99.2	109.5	123.8
4	105.5	115.2	130.0
5	111.5	120.4	135.5
6	118.7	128.0	140.8
7	125.4	134.4	144.3
8	129.1	136.0	148.9
9	136.0	141.2	152.6

3.4. Conclusion

The current article compares the new CRAFTI method against the "gold standard" IMS method and EHSS based computations for quantitative estimation of CCS for prototype aminoalkane- crown ether complexes. Despite differing in absolute CCS values, strong linear correlations were observed between the methods, which serve as a proof of concept for CRAFTI and can be further utilized for validation and calibration. The CRAFTI method was found to be analytically sensitive to increasing cross sections with crown ether ring size and alkylammonium chain length. CRAFTI was also able to distinguish between the normal and branched structural isomers of butylamine.

3.5 References

1. Foye, W. O.; Lemke, T. L.; Williams, D. A., *Foye's principles of medicinal chemistry*. Lippincott Williams & Wilkins: 2008.

2. (a) Miri, R.; Nejati, M.; Saso, L.; Khakdan, F.; Parshad, B.; Mathur, D.; Parmar, V. S.; Bracke, M. E.; Prasad, A. K.; Sharma, S. K., Structure–activity relationship studies of 4-methylcoumarin derivatives as anticancer agents. *Pharm. Biol.* **2016,** *54* (1), 105-110; (b) Sharma, S.; Singh, J.; Ojha, R.; Singh, H.; Kaur, M.; Bedi, P.; Nepali, K., Design strategies, structure activity relationship and mechanistic insights for purines as kinase inhibitors. *Eur. J. Med. Chem.* **2016,** *112*, 298-346.

3. (a) Ferguson, C. N.; Gucinski-Ruth, A. C., Evaluation of Ion Mobility-Mass Spectrometry for Comparative Analysis of Monoclonal Antibodies. *J. Am. Soc. Mass Spectrom.* **2016**, 1-12; (b) Lee, H. H.; Hong, A.; Cho, Y.; Kim, S.; Kim, W. J.; Kim, H. I., Structural Characterization of Anticancer Drug Paclitaxel and Its Metabolites Using Ion Mobility Mass Spectrometry and

Tandem Mass Spectrometry. *J. Am. Soc. Mass Spectrom.* **2016,** *27* (2), 329-338; (c) Reading, E.; Munoz-Muriedas, J.; Roberts, A. D.; Dear, G. J.; Robinson, C. V.; Beaumont, C., Elucidation of drug metabolite structural isomers using molecular modelling coupled with ion mobility mass spectrometry. *Anal. Chem.* **2016**.

4. (a) Jurneczko, E.; Barran, P. E., How useful is ion mobility mass spectrometry for structural biology? The relationship between protein crystal structures and their collision cross sections in the gas phase. *Analyst* **2011,** *136* (1), 20-28; (b) Ruotolo, B. T.; Benesch, J. L.; Sandercock, A. M.; Hyung, S.-J.; Robinson, C. V., Ion mobility–mass spectrometry analysis of large protein complexes. *Nat. Protoc.* **2008,** *3* (7), 1139-1152; (c) Clemmer, D. E.; Jarrold, M. F., Ion mobility measurements and their applications to clusters and biomolecules. *J. Mass Spectrom.* **1997,** *32* (6), 577-592.

5. Merenbloom, S. I.; Flick, T. G.; Williams, E. R., How hot are your ions in TWAVE ion mobility spectrometry? *J. Am. Soc. Mass Spectrom.* **2012,** *23* (3), 553-562.

6. Smith, D. P.; Knapman, T. W.; Campuzano, I.; Malham, R. W.; Berryman, J. T.; Radforda, S. E.; Ashcrofta, A. E., Deciphering drift time measurements from travelling wave ion mobility spectrometry-mass spectrometry studies. *Eur. J. Mass. Spectrom.* **2009,** *12* (13), 13.

7. (a) Yang, F.; Voelkel, J. E.; Dearden, D. V., Collision cross sectional areas from analysis of fourier transform ion cyclotron resonance line width: a new method for characterizing molecular structure. *AnaCh* **2012,** *84* (11), 4851-4857; (b) Yang, F.; Jones, C. A.; Dearden, D. V., Effects of kinetic energy and collision gas on measurement of cross sections by Fourier transform ion cyclotron resonance mass spectrometry. *Int. J. Mass spectrom.* **2015,** *378*, 143-150.

8. Jiang, T.; Chen, Y.; Mao, L.; Marshall, A. G.; Xu, W., Extracting biomolecule collision cross sections from the high-resolution FT-ICR mass spectral linewidths. *Phys. Chem. Chem. Phys.* **2016,** *18* (2), 713-717.

9. Jones, C. A. Ion Structure and Energetics in the Gas Phase Characterized Using Fourier Transfom Ion Cyclotron Resonance Mass Spectrometry. Brigham Young University, 2014.

10. David, W. M.; Brodbelt, J. S., Threshold dissociation energies of protonated amine/polyether complexes in a quadrupole ion trap. *J. Am. Soc. Mass Spectrom.* **2003,** *14* (4), 383-392.

11. (a) Lee, S.; Wyttenbach, T.; von Helden, G.; Bowers, M. T., Gas phase conformations of Li+, Na+, K+, and Cs+ complexed with 18-crown-6. *J. Am. Chem. Soc.* **1995,** *117* (40), 10159-10160; (b) von Helden, G.; Wyttenbach, T.; Bowers, M. T., Conformation of macromolecules in the gas phase: use of matrix-assisted laser desorption methods in ion chromatography. *Sci* **1995,** *267* (5203), 1483; (c) Creaser, C. S.; Griffiths, J. R.; Stockton, B. M., Gas-phase ion mobility studies of amines and polyether/amine complexes using tandem quadrupole ion trap/ion mobility spectrometry. *Eur. J. Mass Spectrom.* **2000,** *6* (2), 213-218; (d) Kralj, M.; Tušek-Božić, L.; Frkanec, L., Biomedical potentials of crown ethers: prospective antitumor agents. *Chem. Med. Chem.* **2008,** *3* (10), 1478-1492.

12. Alizadeh, N.; Shahdousti, P.; Nabavi, S.; Tabrizchi, M., Atmospheric pressure gas-phase ammonium/alkyl ammonium exchange studies of some crown ethers complexes using ion mobility spectrometry: A thermodynamic investigation and collision cross section measurements. *Int. J. Mass spectrom.* **2011,** *308* (1), 18-25.

13. (a) Caravatti, P.; Allemann, M., The 'infinity cell': A new trapped-ion cell with radiofrequency covered trapping electrodes for fourier transform ion cyclotron resonance mass spectrometry. *Org. Mass Spectrom.* **1991,** *26* (5), 514-518; (b) Sievers, H. L.; Grützmacher, H.-F.; Caravatti, P., The geometrical factor of infinitely long cylindrical ICR cells for collision energy-resolved mass spectrometry: appearance energies of EI 2+(E= P, As, Sb, and Bi) from collision-induced dissociation of EI 3+ and [EI 2· ligand]+ complexes. *Int. J. Mass spectrom.* **1996,** *157*, 233-247.

14. Wigger, M.; Nawrocki, J. P.; Watson, C. H.; Eyler, J. R.; Benner, S. A., Assessing enzyme substrate specificity using combinatorial libraries and electrospray ionization-Fourier transform ion cyclotron resonance mass spectrometry. *Rapid Commun. Mass Spectrom.* **1997,** *11*, 1749-1752.

15. Blakney, G. T.; Hendrickson, C. L.; Marshall, A. G., Predator data station: A fast data acquisition system for advanced FT-ICR MS experiments. *Int. J. Mass spectrom.* **2011,** *306* (2), 246-252.

16. Jiao, C. Q.; Ranatunga, D. R. A.; Vaughn, W. E.; Freiser, B. S., A pulsed-leak valve for use with ion trapping mass spectrometers. *J. Am. Soc. Mass Spectrom.* **1996,** *7* (1), 118-122.

17. Jones, C. A.; Dearden, D. V., Linewidth Pressure Measurement: A New Technique for High Vacuum Characterization. *J. Am. Soc. Mass Spectrom.* **2015,** *26* (2), 323-329.

18. (a) Mesleh, M.; Hunter, J.; Shvartsburg, A.; Schatz, G.; Jarrold, M., Structural information from ion mobility measurements: effects of the long-range potential. *J. of Phys. Chem.* **1996,** *100* (40), 16082-16086; (b) Shvartsburg, A. A.; Jarrold, M. F., An exact hard-spheres scattering model for the mobilities of polyatomic ions. *CPL* **1996,** *261* (1), 86-91; (c) Shvartsburg, A. A.; Hudgins,

R. R.; Dugourd, P.; Jarrold, M. F., Structural elucidation of fullerene dimers by high-resolution ion mobility measurements and trajectory calculation simulations. *J. of Phys. Chem. A* **1997,** *101* (9), 1684-1688; (d) Shvartsburg, A. A.; Pederson, L. A.; Hudgins, R. R.; Schatz, G. C.; Jarrold, M. F., Structures of the clusters produced by laser desorption of fullerenes:[2+ 2] cycloadducts of preshrunk cages. *J. of Phys. Chem. A* **1998,** *102* (41), 7919-7923; (e) Shvartsburg, A. A.; Mashkevich, S. V.; Baker, E. S.; Smith, R. D., Optimization of algorithms for ion mobility calculations. *J. of Phys. Chem. A* **2007,** *111* (10), 2002-2010.

19. Maleknia, S.; Brodbelt, J., Cavity-size-dependent dissociation of crown ether/ammonium ion complexes in the gas phase. *J. Am. Chem. Soc.* **1993,** *115* (7), 2837-2843.

Chapter 4 Collision Cross Sections for 20 Protonated Amino Acids: Fourier Transform Ion Cyclotron Resonance and Ion Mobility Result

Disclaimer: This chapter is reproduced from a published research article: Anupriya, Chad A. Jones and David V. Dearden, Collision Cross Sections for 20 Protonated Amino Acids: Fourier Transform Ion Cyclotron Resonance and Ion Mobility Results. Journal of the American Society for Mass Spectrometry DOI:10.1007%2Fs13361-016-1409-x

4.1 Abstract

We report relative dephasing cross sections for the 20 biogenic protonated amino acids measured using the cross sectional areas by Fourier transform ion cyclotron resonance ("CRAFTI") technique at 1.9 keV in the laboratory reference frame, as well as momentum transfer cross sections for the same ions computed from Boltzmann-weighted structures determined using molecular mechanics. Cross sections generally increase with increasing molecular weight. Cross sections for aliphatic and aromatic protonated amino acids are larger than the average trend, suggesting these side chains do not fold efficiently. Sulfur-containing protonated amino acids have smaller than average cross sections, reflecting the mass of the S atom. Protonated amino acids that can internally hydrogen bond have smaller than average cross sections, reflecting more extensive folding. The CRAFTI measurements correlate well with results from drift ion mobility (IMS) and traveling wave ion mobility (TWIMS) spectrometric measurements; CRAFTI results correlate with IMS values approximately as well as IMS and TWIMS values from independent measurements correlate with each other. Both CRAFTI and IMS results correlate well with the computed momentum transfer cross sections, suggesting both techniques provide accurate molecular structural information. Absolute values obtained using the various methods differ significantly; in the case of CRAFTI, this may be due to errors in measurements of collision gas

pressure, measurement of excitation voltage, and/or dependence of cross sections on kinetic energy.

4.2 Introduction

We recently introduced a new method for measuring ion dephasing cross sections using Fourier transform ion cyclotron resonance (FTICR) mass spectrometry.[1] The method is based on measuring the rate of ion loss from the coherently-orbiting ion packet prepared after an FTICR excitation, and we refer to it by the acronym "CRAFTI" (cross sectional areas by Fourier transform ion cyclotron resonance). Essentially the same method, although employing different data analysis techniques, has recently been applied to larger biomolecular ions such as ubiquitin and cytochrome c.[2] Although relative CRAFTI cross sections have been shown to correlate with measurements made using drift ion mobility spectrometry (IMS) and with momentum transfer cross sections calculated from molecular models,[1a] absolute agreement between CRAFTI cross sections and IMS results is generally poor due to the significant differences between the techniques: CRAFTI involves single, high energy collisions between ions and (typically) neutral Ar atoms, whereas IMS involves multiple, essentially thermal collisions between ions and (typically) He or N_2.

As the building blocks of proteins, the 20 biogenic amino acids are among the most important biomolecules and their fundamental chemistry has attracted a great deal of attention over the years. The mobilities of the protonated biogenic amino acid ions have been reported at least three times,[3] and cross sections for an abbreviated set examined using traveling wave ion mobility spectrometry (TWIMS) have also been reported.[4] Mobilities for a set of abiogenic amino acids, which showed a correlation between molecular weight and mobility, have also appeared.[5]

Because they are well-characterized small molecules and represent a set of diverse molecular structures, the protonated amino acids are ideal for examining the utility of CRAFTI

measurements for characterizing molecular structure. We have therefore converted the reported mobilities of the protonated amino acids to collision cross sections for comparison with measured CRAFTI cross sections, which can now be determined more accurately and with greater precision because of a new method for measuring pressures in the FTICR trapping cell.[6] We also report momentum transfer cross sections calculated from molecular modeling, and compare the computational results with the experimentally measured values to extract structural insights about the protonated amino acids.

4.3 Experimental

4.3.1 Materials

Amino acids were purchased from Sigma-Aldrich (St. Louis, MO) and used without further purification. Electrospray samples were prepared by first dissolving in 88% formic acid (Mallinckrodt Baker Inc., Phillipsburg, NJ) and then diluting with methanol/water (50:50) to a final concentration of 100-200 μM. Argon gas was purchased from Airgas (Radnor, PA) at a purity of 99.995%.

4.3.2 Instrumentation

All experiments were conducted using a Bruker model APEX 47e Fourier transform ion cyclotron resonance mass spectrometer controlled by a MIDAS Predator[7] data system and equipped with an infinity cell[8] and a 4.7 T superconducting magnet. Ions were generated in a microelectrospray source modified from an Analytica (Branford, MA) design, with a heated metal capillary drying tube based on the design of Eyler.[9] The instrument was equipped with a Freiser-type[10] pulsed leak valve consisting of a 0.004" orifice pressurization solenoid valve backed by a 28 psig Ar supply line and a 0.039" orifice evacuation solenoid valve connected to a mechanical vacuum pump (both valves from General Valve Corp.; Fairfield, NJ). Both solenoid valves were

connected to the high-pressure side of a precision variable leak valve (Varian; Palo Alto, CA); the volume of the "valve space" between the two solenoid valves was approximately 4 mL. Steady-state pressures obtained with the pulsed leak system were varied by varying the length of time the pressurization solenoid valve was left open (while the evacuation solenoid is left closed). The operation and performance characteristics of our pulsed leak valve have been described in more detail elsewhere.[6]

4.3.3 Procedures

RF excitation amplitudes were measured with an oscilloscope at the output of the final excitation amplifier, and were also characterized by measuring the excitation amplitudes required to eject ions from the trap at various excitation durations. These two methods give slightly different absolute peak-to-peak voltages, but exhibit excellent linear correlation with each other ($R^2 > 0.99$).

Absolute pressures were measured by measuring Ar^+ linewidths in Ar background gas as described in detail elsewhere.[6] Briefly, the linewidth of Ar^+ in neutral Ar was measured for each of the pulsed leak valve pressurization durations. Ar^+ in Ar momentum transfer cross sections from the literature[11] enable calculation of the absolute pressure from the measured linewidths. Pressures measured in this way[6] are calibrated for Ar and so are not subject to uncertainty from chemical sensitivity, and are measured in the trapping cell so are not subject to errors resulting from measurement at a point remote from the trapping cell. They do not involve ion current measurements, so are not adversely affected by the magnetic field. These pressure measurements were performed both before and after each amino acid cross section measurement. The average pressure was used in determining the amino acid CRAFTI cross section, although pressure drifts were generally less than 2×10^{-9} mbar.

The procedure for the cross section measurements is described in detail elsewhere.[1a] Briefly, protonated amino acid ions were generated via electrospray and injected into the FTICR trapping cell. No attempt was made to maintain constant ion abundances from one measurement to the next, aside from assuring strong signal was always present in each experiment. Next, the ions were monoisotopically isolated using SWIFT techniques,[12] followed by pulsing Ar into the FTICR trapping cell to a constant pressure using the pulsed leak valve, waiting for 3 sec to allow collisional damping of any residual excitation from the SWIFT event, then exciting the ions via a single-frequency pulse at their resonant cyclotron frequency for 350 μsec with an amplitude appropriate to achieve the desired kinetic energy (in this case, a laboratory frame energy of 1.9 keV, a value arbitrarily chosen because it allowed collection of strong signal for all of the target ions with a short excitation event). The short excitation event minimizes the probability of collisions occurring during the excite, although experiments performed with different excite amplitudes and durations that each result in the same net excitation show only small, random variation in the measured cross sections, even at the highest pressures used, suggesting that under the conditions employed collisions during the excitation are not significant.

The resulting time domain image current signal yields a frequency domain power spectrum after Fourier transformation with one zero fill and no apodization; typically, about 10 scans were averaged for each spectrum. A set of power spectral full width at half maximum linewidths measured at various Ar pressures is collected. Plots of linewidths vs. collision gas number density are generally linear, and the slope is used to determine the CRAFTI cross section. Experimental results were processed using the Igor Pro software package (version 6.34A, Wavemetrics; Lake Oswego, OR).

4.3.4 Computational Modeling

Molecular structures were obtained using the Spartan '08 package (Wavefunction, Inc.**;** Irvine, CA) for conformational searching using the MMFF force field provided in the package, requesting 10,000 starting conformers (but systematic searches sometimes completed after examining fewer than 10,000 structures). In each case, the amino acid was protonated on the amine group. For each protonated amino acid, the five conformers with the lowest MMFF energies were analyzed using the MOBCAL package[13] and their momentum transfer collision cross sections were computed using the projection approximation, using the exact hard sphere scattering method, and using the trajectory method as implemented in MOBCAL. MOBCAL assumes the neutral collision gas is He. The resulting cross sections for these lowest-energy conformers were then weighted using a 300 K Boltzmann distribution function and averaged. We justify this averaging by noting that none of the techniques used for experimentally measuring the cross sections have sufficient resolution to resolve the different conformers that may be present for a given amino acid; in particular, the experimental arrival time distributions in the literatur[3a, 3b] show single peaks for each amino acid. A similar averaging approach has been used previously.[4]

4.4 Results

4.4.1 Collision cross sections of protonated amino acids

Cross sections for 20 singly-protonated amino acid ions, measured using CRAFTI at a kinetic energy of 1.9 keV in the laboratory reference frame, are listed in Table 3.1 Cross sections (Å2) for protonated crown ether-alkyl monoamine complexes using CRAFTI., along with values computed from previously reported[3] reduced mobilities, values measured using TWIMS,[4] and values from MOBCAL exact hard sphere scattering (EHS) calculations performed as described above (the MOBCAL projection approximation and trajectory methods give results quite similar

to those of the EHS calculations, but we focus on EHS values because the CRAFTI experiments are conducted at energies where the hard sphere potential is probably the best description of the interaction between the neutral collision gas and the ion). The values from references [3] were calculated from the reduced ion mobilities reported therein using Equation 4-1.[14]

$$\Omega = \frac{3ze}{16N_0}\left(\frac{2\pi}{\mu kT}\right)^{1/2}\frac{1}{K_0} \tag{4-1}$$

Here, Ω is the momentum transfer cross section, z is the charge on the ion, e is the elementary charge, N_0 is the number density of an ideal gas at a pressure of 1 atm, μ is the reduced mass of the collision system, k is Boltzmann's constant, T is the absolute temperature, and K_0 is the reduced mobility.

A few trends are evident from the table. First, with a spread of over 200 Å^2, the CRAFTI results span a much larger range of values than any set of IMS measurements (each of the IMS measurements of the 20 amino acids spans less than 30 Å^2 in total spread). Next, examining the IMS data, cross sections measured in Ar are smaller than those measured in N_2, whereas those measured in CO_2 are larger than those measured in N_2. This is consistent with what would be expected based on the relative sizes of the collision gases. With the exception of the TWIMS results, all of the experimental values are larger than the computed cross sections.

Table 4.1 Cross sections ($Å^2$) for protonated amino acids in various collision gases.

Amino acid	Molecular Weight, Da	EHS Scattering Calculation He	IMS (collision gas, field (V cm^{-1})) N_2, 3c	200N_2, 3b	269N_2, 3a	280N_2, 3b	347Ar, 3b	284CO_2, 3b	TWIMS 387He 4	CRAFTI Ar
glycine	76.0399	48.8	107.5	96.5	90.9	96.6	88.8	140.3	-	51.7 ± 1.3
alanine	90.0555	54.5	106.9	100.7	97.0	95.9	85.5	135.7	-	71.4 ± 0.7
serine	106.0504	57.7	107.9	99.0	94.5	99.1	87.3	140.4	-	85.1 ± 0.8
proline	116.0785	62.7	107.3	100.4	95.3	100.7	89.5	137.8	62.43	102.1 ± 1.2
valine	118.0868	65.1	111.5	103.4	98.8	103.8	94.6	142.8	64.81	113.4 ± 0.3
threonine	120.0655	63.1	109.7	101.1	96.6	100.8	89.2	141.2	-	106.1 ± 2.0
cysteine	122.0270	60.7	110.4	103.0	97.0	104.0	-	-	-	101.0 ± 0.4
isoleucine	132.1025	70.7	-	106.1	103.1	106.3	99.9	143.0	68.95	133.1 ± 1.2
leucine	132.1025	72.3	116.7	109.9	104.0	110.3	101.4	147.5	70.51	138.9 ± 1.0
asparagine	133.0608	65.6	111.2	102.8	98.1	103.3	90.5	143.2	-	124.8 ± 0.9
aspartic acid	134.0448	64.5	113.0	103.8	98.7	104.0	90.8	144.5	62.93	124.0 ± 1.5
glutamine	147.0764	71.0	112.9	104.7	101.8	105.1	97.3	142.2	62.85	146.9 ± 1.5
lysine	147.1128	74.3	113.0	108.7	104.1	108.7	98.3	140.5	-	153.8 ± 1.0
glutamic acid	148.0740	70.2	113.9	105.9	101.4	106.5	97.5	143.9	63.35	152.3 ± 0.4
methionine	150.0589	72.7	115.2	107.5	104.3	107.7	96.9	144.1	-	148.9 ± 1.9
histidine	156.0767	73.5	113.6	107.2	103.3	107.8	95.6	142.7	-	153.6 ± 1.3
phenylalanine	166.0862	79.8	121.6	114.0	110.6	114.2	106.9	151.1	-	183.3 ± 0.9
arginine	175.1189	79.1	118.1	114.7	109.6	113.4	101.8	146.1	-	190.3 ± 1.4
tyrosine	182.0920	83.6	127.4	120.0	114.1	120.2	110.1	149.7	-	211.5 ± 2.1
tryptophan	205.0971	89.7	129.8	123.9	120.8	124.3	115.6	160.8	-	256.4 ± 0.7

4.5 Discussion

In the discussion that follows, we first examine the structural differences among the protonated amino acids that can be gleaned from the cross section results. Since the goal of most cross section experiments is to distinguish among structural possibilities by comparison with computational results, we next examine the correlation between the experimental results and the conformationally averaged computed cross sections. We will show that each of these comparisons suggests CRAFTI measurements detect differences in molecular structure in the gas phase. Finally, we discuss possible explanations for why the CRAFTI cross sections are not in good quantitative agreement with the computed values.

4.5.1 Structural information for protonated amino acids from cross sections

Cross sections computed using exact hard sphere scattering, and measured using CRAFTI in Ar at 1.9 keV in the laboratory frame and using IMS in N_2 with a 269 V cm^{-1} drift field[3b] for the 20 protonated amino acids are plotted vs. molecular weight in Figure 4.1. This set of IMS values are shown because they are from the most recent publication that includes all 20 amino acids and because the field strength is intermediate between the field strengths used for the other reported IMS measurements. As expected, cross sections generally increase with molecular weight. However, deviations from this general trend, arising from structural differences in the protonated amino acids, are seen as patterns in the data. Strikingly, *almost identical patterns in these deviations are evident in the calculated results and in both experimental data sets*. This strongly suggests that CRAFTI is sensitive to molecular structure in much the same way as IMS, and that both experimental methods reflect structural trends also captured by the calculations.

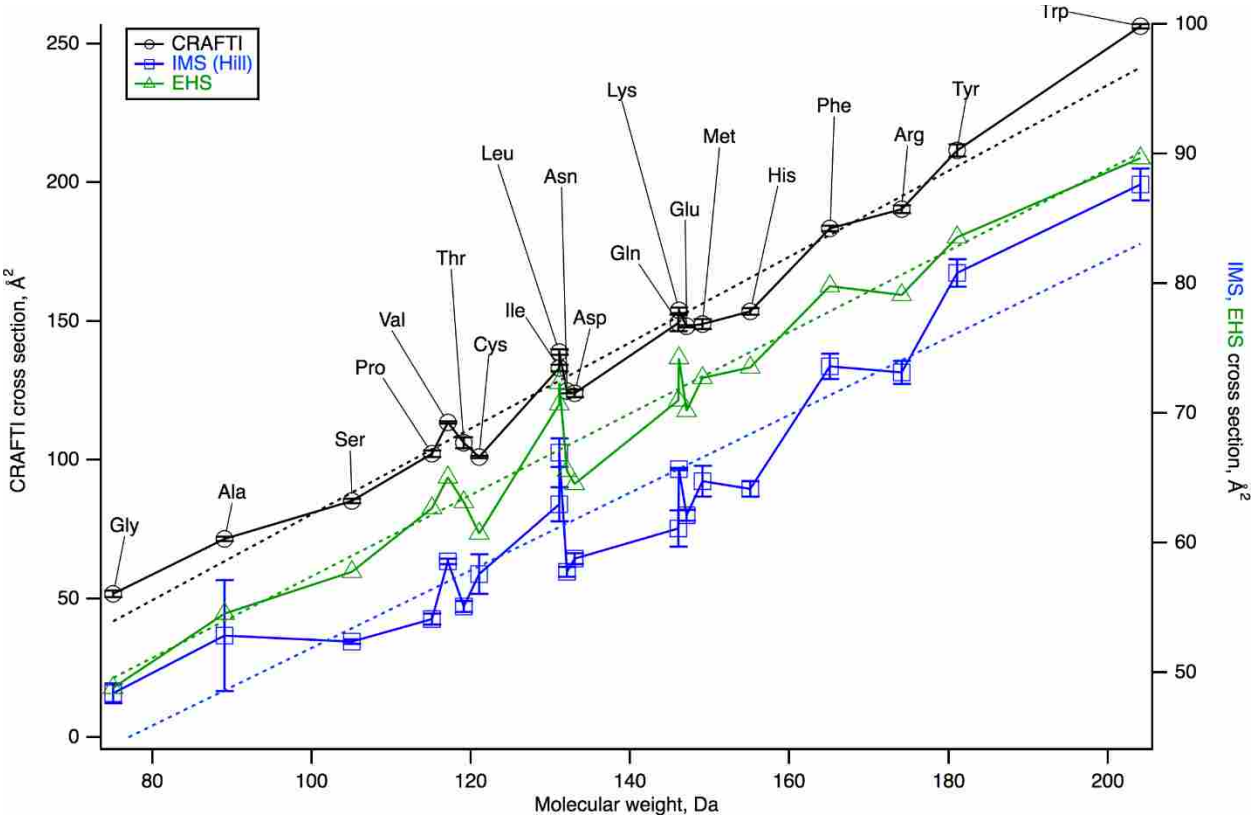

Figure 4.1 Cross sections for 20 protonated amino acids computed using exact hard sphere scattering theory (EHS), and measured using CRAFTI in Ar at 1.9 keV in the lab frame or ion mobility spectrometry in N_2 with a 269 V cm^{-1} drift field,[3b] plotted as a function of molecular weight. Lines between data points serve only to guide the eye and make patterns in the data evident. Dotted lines are linear fits to each data set. Error bars represent one standard deviation from replicate measurements (CRAFTI) or from replicate published measurements (IMS). Note that the CRAFTI data reference the left axis, whereas the EHS and IMS data reference the right axis

4.5.1.1 Compactness of protonated amino acids in the gas phase

The general correlation between cross section and molecular weight has been noted previously,[5] and is clearly evident in all three data sets. Unsurprisingly, higher molecular weights generally indicate more atoms and correspondingly larger cross sections. The linear fits plotted as dotted lines in Figure 4.1 represent the average variation in cross section with mass for the protonated amino acids, determined using each method. Deviations from this general trend are of particular interest, and are the focus of the following discussion.

The aliphatic amino acids Ala, Val, Leu, and Ile all have cross sections that are greater than the average trend line in all three data sets, suggesting that aliphatic side chains do not fold as compactly as in the average amino acid. This reflects the weaker dispersion and ion-induced dipole interactions that dominate for these nonpolar side chains. This observation has been made previously for the TWIMS data.[4] Similarly, the aromatic amino acids Phe and Tyr both have cross sections greater than predicted for the average amino acid in all three data sets, suggesting that aromatic side chains do not fold as compactly as the average side chain, perhaps because of weaker interactions and the high rigidity of aromatic substituents.

The sulfur-containing amino acids Cys and Met each have cross sections below the average trendline in all three data sets. The relatively small cross sections for Cys and Met likely reflect the fact that the heavy sulfur atom adds mass to the amino acid without adding as much bulk as, for example, two lighter oxygen atoms would add. The effect of the sulfur atom is evident when sulfur is substituted for oxygen, as in comparing Ser and Cys: the sulfur atom leads to a larger cross section for Cys, probably both because the S atom is larger than O and because less internal hydrogen bonding is possible for the thiol in Cys than for the alcohol group in Ser.

The effects of internal hydrogen bonding, which have been noted previously in the TWIMS study,[4] can be examined by comparing Val, which has an aliphatic side chain that cannot hydrogen

bond effectively, with Thr, which has a side chain of the same length and shape but that can hydrogen bond through its OH group. Both the CRAFTI and IMS data and the computational results indicate that the cross section of Thr is smaller than that of Val, suggesting that internal hydrogen bonding enables more compact folding of the side chain in this case. Similarly, Asn, Asp, Gln, Glu, His, and Arg, all of which can internally hydrogen bond, all have cross sections less than the average trend in all three data sets. This is especially the case for His, which of course has a cyclic side chain and would therefore be expected to be compact. Interestingly, the cross section of protonated Lys is on or slightly above the average trend line, despite the presumed ability of its long, basic side chain to internally hydrogen bond. Perhaps the ring that would result, which would be at least 8-membered, is too large to allow optimal internal H-bonding or compact folding.

The three data sets disagree about whether protonated Cys has a larger cross section than protonated Thr; CRAFTI and EHS indicate Cys is smaller, whereas IMS has Cys larger. Both these amino acids have side chains 2 heavy atoms long, although the Thr side chain includes a branch (which would tend to increase the cross section). On the other hand, the OH group of Thr is capable of internal hydrogen bonding with both the ammonium and acid groups (which would tend to decrease the cross section), whereas that tendency is much less for the SH of Cys. Thus, it is difficult to decide which data set provides a more accurate description.

4.5.1.2 Distinguishing isomeric and isobaric structures

All three data sets compared in Figure 4.1, and the TWIMS results as well (Table 3.1 Cross sections (Å2) for protonated crown ether-alkyl monoamine complexes using CRAFTI.), indicate that Leu has a significantly larger cross section than Ile; placement of the side chain's methyl branch closer to the main amino acid chain is inherently more compact. Similarly, Gln and Lys, which at m/z 147.077 and 147.113, respectively, are nearly isobaric, can be distinguished on the

basis of a larger cross section for Lys; the longer Lys side chain probably explains the difference. Unfortunately, it is likely that mixtures of these isomeric or isobaric amino acids will be problematic in practical measurements because neither CRAFTI, IMS, nor TWIMS (as they are currently practiced) has sufficient resolving power to separate species with such similar cross sections.

In summary, CRAFTI measurements show the same structural trends that are evident in the EHS calculations and in the IMS cross sections. These structural trends are consistent with expectations based on the intramolecular interactions within the protonated amino acids, suggesting that CRAFTI, like IMS, can be used to deduce structural information. Our confidence in such conclusions is increased by the strong qualitative agreement between the different, independent methods.

4.5.2 Correlation of experimental cross sections with cross sections computed using the exact hard sphere scattering method

One of the great merits of ion mobility measurements is that cross sections derived from mobilities have been shown to correlate with molecular structure, so mobility measurements can be used to obtain structural information. CRAFTI cross sections should correlate with molecular structure if CRAFTI is to have analytical value. One means of evaluating the utility of CRAFTI measurements for obtaining structural information is to examine how they correlate with cross sections computed from structures derived from molecular modeling. This is especially appropriate given that one of the most important applications of cross section measurements is to distinguish between candidate molecular structures or conformers, which usually originate from molecular modeling. The correlation of the experimental data sets with Boltzmann-weighted average EHS cross sections is shown in Figure 4.2, with parameters obtained from the fits

compiled in Table 4.2 Results for fits of experimental IMS and CRAFTI cross sections vs. cross sections calculated with the MOBCAL EHS method.

Inspection of Figure 4.2 and Table 4.2 Results for fits of experimental IMS and CRAFTI cross sections vs. cross sections calculated with the MOBCAL EHS method shows that the correlation lines for most of the IMS data sets have similar slopes, but none are within experimental error of the "ideal" value of 1. Similarly, none of the intercepts is within experimental error of zero. Strikingly, the slope for the CRAFTI correlation curve is much greater than those for the IMS data, and the intercept is far from zero. We will discuss possible explanations below.

None of the experimental data sets (except the TWIMS data,[4] which were calibrated to agree) agrees particularly well with the computed EHS cross sections, although the absolute agreement is better for the IMS results than for CRAFTI. In fact, it is a little puzzling that the IMS results do not agree more closely with the calculations, because the MOBCAL trajectory method calculation is designed and calibrated to reproduce IMS results. The exact reasons for this disagreement are not clear, but some disagreement is expected because the calculations assume He collision gas and none of the experiments were done in He. However, we note that the *correlation* between either IMS or CRAFTI experimental results and the EHS calculations is very good (*vide infra*) such that either type of experimental result could easily be calibrated to yield results in close agreement with the EHS calculations. Although the absolute agreement is poor, the observed trends in the CRAFTI data correlate quite well with the computed cross sections, as discussed below.

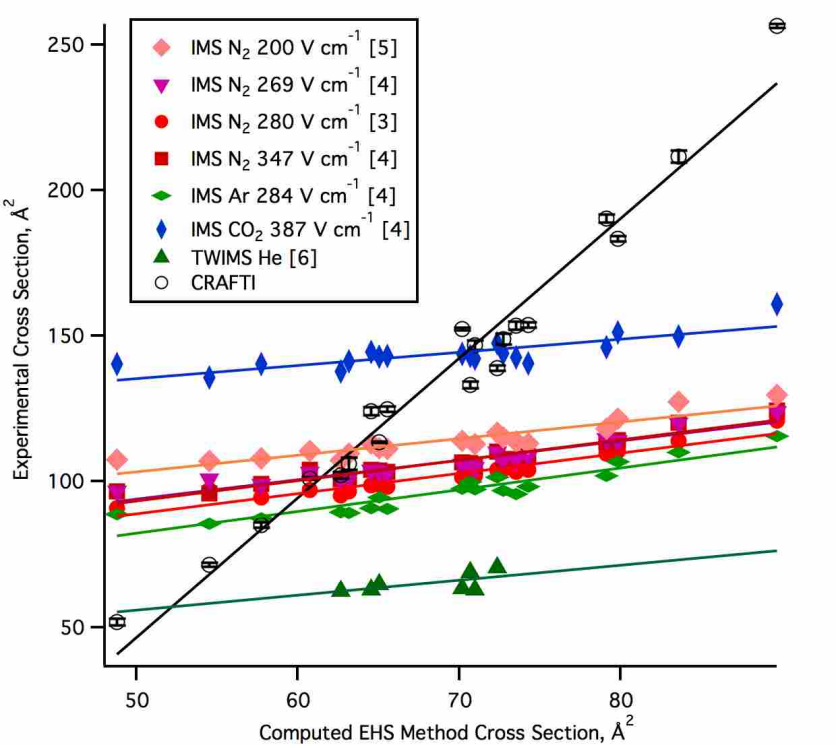

Figure 4.2 Correlation of experimental cross section measurements with Boltzmann-weighted cross sections computed using the exact hard sphere scattering method from molecular models. Error bars represent ± 1 standard deviation from replicate measurements, and lines are linear fits to the data; references for literature data are shown in the symbol key

Table 4.2 Results for fits of experimental IMS and CRAFTI cross sections vs. cross sections calculated with the MOBCAL EHS method

Experimental conditions[1]	Intercept	Slope	R^2 [2]
IMS N_2, 200 V cm^{-1} [3c]	74 ± 4	0.57 ± 0.06	0.824
IMS N_2, 268.9 V cm^{-1} [3b]	61 ± 4	0.67 ± 0.05	0.879
IMS N_2, 280 V cm^{-1} [3a]	54 ± 3	0.70 ± 0.05	0.905
IMS N_2, 346.9 V cm^{-1} [3b]	58 ± 3	0.70 ± 0.05	0.904
IMS Ar, 284.4 V cm^{-1} [3b]	45 ± 5	0.75 ± 0.07	0.838
IMS CO_2, 386.7 V cm^{-1} [3b]	113 ± 5	0.45 ± 0.08	0.678
TWIMS He [7]	30 ± 21	0.52 ± 0.30	0.371
CRAFTI Ar, 1.9 keV	-193 ± 14	4.80 ± 0.20	0.978

[1] For literature IMS data sets, these are drift gas and drift field strength. For CRAFTI data, collision gas and laboratory frame collision energy

[2] Boltzmann weighted average of 5 lowest MMFF energy conformers computed using the trajectory method in MOBCAL

Even though none of the experimental data sets agree perfectly with the calculated results, all show reasonable linear correlations with the calculated results. Perhaps surprisingly, the correlation between the CRAFTI data and the EHS cross sections is somewhat better (as measured via R^2, Table 4.2 Results for fits of experimental IMS and CRAFTI cross sections vs. cross sections calculated with the MOBCAL EHS method) than the correlation observed for any of the IMS data sets,[3] despite the fact that the computed cross sections were designed to reproduce IMS results. The same is true when the various experimental measurements are correlated with either the projection approximation or trajectory method calculations (data not shown), so this is not an artifact due to using the EHS method. The correlation between the TWIMS data and the computed cross sections is weaker, but the trend line for the TWIMS data is quite similar to that observed for the full IMS data sets and likely the weaker correlation is just due to fewer points in the TWIMS data.

In some cases, the deviations for all the experimental measurements from the best-fit lines are similar. For example, the experimental cross section for the smallest protonated amino acid, $GlyH^+$, is above the trendline in every dataset. Similarly, the experimental values for the largest protonated amino acid, $TrpH^+$, are above the trendlines in every dataset. Results such as these suggest that perhaps the error actually lies in the model calculation, and point out an additional benefit of having an additional, independent means, such as CRAFTI, of making the experimental measurements.

The correlation between experimental and computed cross sections improves slightly for each of the experimental methods when Boltzmann-weighted average computed cross sections are used, rather than simply using the computed cross sections for the lowest-energy structures found in the MMFF conformational search for each amino acid. Evidently the averaging procedure helps

make up for likely inaccuracies in the MMFF force field's relative energies for the various conformers.

In summary, all the experimental measurements correlate linearly with the Boltzmann-weighted average computed EHS cross sections, so results from any of these experimental methods could be linearly scaled to produce results that compare quantitatively with the computed values. This is already routinely done in the calibration of TWIMS measurements, and the excellent correlation between CRAFTI measurements and EHS cross sections suggests a similar procedure could be used with CRAFTI.

4.5.3 Correlation of CRAFTI cross sections with those from mobility methods

The agreement between various experimental cross section measurements for the 20 biogenic protonated amino acids is depicted in Figure 4.3. In the Figure, as above, we have used the IMS values from Reference [3b] measured in N_2 collision gas at a field strength of 269 V cm^{-1} as the baseline values against which the other measurements are compared. Linear fits of the other data sets measured using drift IMS or TWIMS against this baseline set all have slopes with values near 1, although the intercepts of these fits are all significantly different from 0. The other data sets measured in N_2 collision gas correlate well with the baseline set; the correlation coefficients, R^2, are 0.95 or greater in each case. The correlations are weaker for IMS measurements performed in Ar or CO_2 collision gases, with R^2 values of 0.917 and 0.765, respectively. TWIMS measurements with He collision gas[4] also correlate less well, with an R^2 value of 0.633, although this may at least in part be due to the fact that only 7 of the 20 protonated amino acids were measured in the TWIMS study.

As expected from the data in Table 3.1 Cross sections (Å2) for protonated crown ether-alkyl monoamine complexes using CRAFTI., the fit of the CRAFTI data against the baseline set

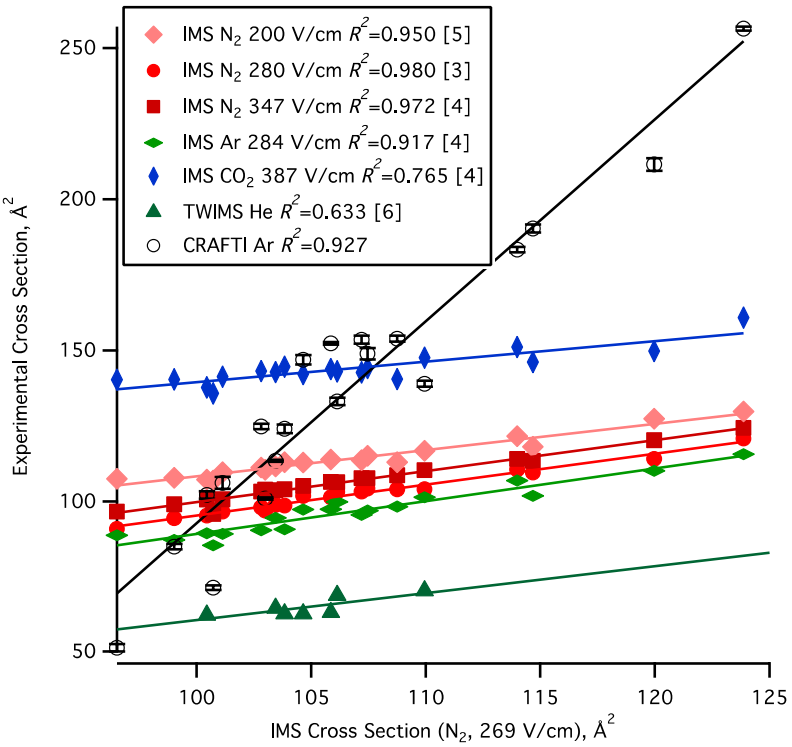

Figure 4.3 Correlation of various protonated amino acid cross section data sets with ion mobility spectrometry (IMS) data measured in N_2 at a 269 V cm^{-1} drift field [3b]. Lines are linear fits to the correlation data; R^2 values for each fit are shown in the symbol key along with references for the literature data

yields a slope much greater than 1 (6.7 ± 0.4). The correlation coefficient from the CRAFTI fit is 0.927, which is comparable to the R^2 value obtained when IMS measurements made with Ar collision gas are compared with those made in N_2. Therefore, even when compared with IMS measurements made at much lower energies in a different collision gas, the CRAFTI values correlate reasonably well.

4.5.4 Disagreement of absolute CRAFTI cross sections with those from mobility methods

Although the qualitative correlation between CRAFTI cross sections and both EHS calculations as well as IMS measurements is very good, strongly suggesting CRAFTI reflects structural differences among the protonated amino acids, the absolute agreement in the values is poor. Our long-range goal is to make accurate absolute cross section measurements using CRAFTI, because such measurements could be compared with cross sections calculated from molecular structures and used to distinguish between different possible structures. This is already done routinely using IMS data and can be done using TWIMS measurements if the TWIMS results are properly calibrated.

The data in Table 3.1 Cross sections (Å2) for protonated crown ether-alkyl monoamine complexes using CRAFTI. show that the absolute agreement between CRAFTI and either computed cross sections or other experimental measurements is poor; CRAFTI cross sections for the smallest protonated amino acids are only slightly larger than the EHS values, whereas most CRAFTI cross sections are much larger than the EHS values and for the most massive ions the CRAFTI cross sections are nearly a factor of 3 larger than those from the EHS calculations. This difference is most easily seen in the very large slope and nonzero intercept of the CRAFTI-EHS correlation line (Figure 4.2 and Table 4.2 Results for fits of experimental IMS and CRAFTI cross sections vs. cross sections calculated with the MOBCAL EHS method).

As we attempt to make comparisons between the absolute values of cross sections made using CRAFTI with those from IMS (and with those from calculations, such as the EHS calculations used here, that are designed to model IMS), we wish to emphasize the significant differences between the techniques. IMS measurements involve multiple low-energy collisions (typically about 0.1 eV) between ions and neutrals; the change in drift time for ions with different cross sections is the cumulative result of a large number of collisions. At these low collision energies, for small molecules such as the protonated amino acids described here, the Langevin ion-induced dipole cross section is larger than the hard sphere cross section, so IMS data will be strongly dependent on the long-range ion-induced dipole interaction potential. CRAFTI, on the other hand, involves single collisions at far higher energies (1.9 keV in the laboratory frame in this work) and detects the collisions by whether or not the ion's motion is dephased from that of the coherently-orbiting packet prepared by the FTICR excitation pulse.

Langevin cross sections decrease with increasing relative velocity. At the energies and velocities used in FTICR detection events, hard sphere cross sections are always larger than Langevin cross sections, so a hard sphere collision model is more appropriate [15]. The influence of collision models on cross section measurements in FTICR instruments, and the importance of making the measurements under "energetic hard sphere" scattering conditions, has recently been discussed [16]. Dephasing will definitely occur if the ion undergoes collision-induced dissociation, which is likely at these energies. Because dissociation changes the cyclotron frequency of the ion, ions that undergo dissociative collisions are no longer part of the coherent packet. Momentum transfer may also cause dephasing, but its role is more complex than in IMS because it is unclear what fraction of the ion's momentum must be lost to cause it to dephase; some collisions could

result in slowing the ion down so that its orbit radius decreases, while leaving it in phase with the rest of the packet.

If momentum transfer were the only process contributing to the CRAFTI cross sections, we would expect the CRAFTI cross sections to be *smaller* than the IMS cross sections, both because we use a smaller collision gas (Ar, vs. N_2 in the relevant IMS cases) and because momentum transfer cross sections decrease with increasing kinetic energy (as we noted above, CRAFTI is carried out at much higher collision energy (1.9 keV in the laboratory frame in these experiments) than IMS (less than 0.1 eV, typically)). In fact, variable-energy CRAFTI experiments conducted with monoatomic ions [6], which cannot dissociate, and with a few of the protonated amino acids (data not shown) do show decreasing cross sections with increasing kinetic energies.

As a reviewer points out, collisions resulting in dissociation should already be included in the hard sphere momentum transfer cross section and so should not cause CRAFTI cross sections to be larger than IMS momentum transfer cross sections. Other processes must therefore play a role in CRAFTI. For instance, it is possible that ion-ion collisions might lead to scattering and dephasing. Ion-ion collision cross sections would be expected to be much larger than hard sphere cross sections. However, we see no evidence of ion-ion collisions; if such processes were dominant we would expect nonlinear dependence of FTICR linewidth on collision gas pressure, which we do not observe. Further, experiments in which CRAFTI cross sections are measured for varying initial signal amplitudes (obtained by de-tuning the ion source) show only random variation in cross section with initial signal amplitude, suggesting ion-ion collisions or space charge effects do not significantly influence the current results.

So what might account for these differences? The equation used to calculate CRAFTI cross sections, σ_{CRAFTI}, is reproduced here:[1]

$$\sigma = \frac{FWHM}{n_n}\frac{(m+M)}{M}\frac{m}{q}\frac{d}{\beta V_{PP} t_{exc}} \quad (4\text{-}2)$$

In Equation 4-2, *fwhm* is the measured full-width at half-maximum power spectral linewidth, n_{neut} is the neutral collision gas number density, m is the mass of the ion, M is the mass of the neutral collision gas, q is the charge of the ion, d is the diameter of the FTICR trapping cell, β is the geometry factor for the trapping cell (0.897 for the Infinity cell used in these experiments [17]), V_{pp} is the peak-to-peak amplitude of the single-frequency RF excitation pulse, and t_{exc} is the duration of that pulse. The derivation of the equation depends on the assumption that single, hard-sphere collisions are sufficient to cause dephasing of ions from the coherently-orbiting packet produced by application of the excitation pulse to the ion population. In the case of the protonated amino acids, the collision gas (Ar, 39 amu) is not much less massive than the ions (76—205 amu), so single, energetic collisions are likely to cause dephasing. In addition, plots of *fwhm* linewidths vs. collision gas pressure are linear, again suggesting we are operating in a regime where ions are dephased by single collisions.

Could errors in one or more of the terms used in the calculation of cross sections account for the disagreements with the IMS results? Most of the terms in (2), including all the masses and charge, are easily and accurately measured. The same trapping cell with the same diameter, *d,* and cell geometry constant, β, and the same value of t_{exc} were used in all experiments; these could not account for the observed differences. The *fwhm* term is experimentally measured, typically with values of tens to hundreds of Hz and with differences between replicate measurements of less than 1%, so is not likely to account for large errors in the absolute cross sections.

This leaves n_{neut} and V_{pp} as potential sources of error. CRAFTI cross sections are inversely dependent on both terms, but because neither term was held constant for all experiments the dependence is more complex than simple inverse dependence. We explored the influence of each

of these terms by means of a spreadsheet model that allowed linear variation of all the n_{neut} or V_{pp} terms so that the effects on the entire CRAFTI dataset could be gauged. Our purpose in doing this is not to force the CRAFTI results into agreement with the other data, but merely to examine how the the n_{neut} and V_{pp} terms affect the results for the entire dataset.

The n_{neut} term is difficult to measure accurately. As noted above, we measure pressures (and therefore the n_{neut} term) by measuring the Ar^+ in Ar FTICR linewidth [6]; the values reported in Table 3.1 Cross sections (Å2) for protonated crown ether-alkyl monoamine complexes using CRAFTI. are all based on such linewidth pressure measurements. We also measured pressures during these experiments using more conventional cold cathode gauge tube methods. These two pressure measurement techniques can differ by as much as a factor of 2. Errors in pressure could well account for large errors in absolute cross sections. If the n_{neut} term is systematically too small, cross sections would be correspondingly too large; a factor of 2 error, which is not unreasonable, would be sufficient to bring the absolute CRAFTI cross sections into rough agreement with the EHS values. Because the pressure variation was different for each amino acid, scaling the pressure affects both the slope and the intercept of the CRAFTI-EHS correlation curve. So, if the pressures derived from Ar^+ in Ar FTICR linewidths were too small by a reasonable factor, that might account for the absolute differences.

The V_{pp} values were measured using an oscilloscope, and varied with the masses of the different amino acids so as to maintain constant laboratory frame kinetic energy. Connection of the scope to the RF circuit changes the impedance of the circuit and could make the results inaccurate. As with the possible pressure errors noted above, linear scaling of the voltages affects both the slope and the intercept of the CRAFTI-EHS correlation curve. If the voltages used in determining the CRAFTI cross sections were systematically too small, this alone could account

for the absolute differences. Again, the range of excitation voltages that produce reasonable agreement is well within the range accessible using our excitation amplifier and so is not unreasonable. Obviously, simultaneous linear variation of both the n_{neut} and the V_{pp} terms allows closer agreement with the EHS values.

One additional factor should be considered. Because the CRAFTI experiments were conducted at constant laboratory frame kinetic energy, collision energies in the center-of-mass reference frame were not constant, in contrast to the near-zero collision energies used in IMS measurements. Rather, collision energies in the center-of-mass frame decreased with increasing ion mass: the center-of-mass energy for the $GlyH^+$ measurements was roughly twice that for the $TrpH^+$ measurements. Because collision cross sections increase with decreasing collision energy, we might expect the cross sections for the higher mass ions to be larger than they would be if all the experiments had been performed at the same energy in the center-of-mass reference frame, and this might account for some of observed deviations. This idea will be tested in future experiments, although at this point it seems unlikely that kinetic energy differences alone could account for all the disagreement.

In summary, at this point it is not clear why the absolute CRAFTI cross sections do not agree better with the absolute values measured using IMS techniques or calculated from conformationally-averaged structures. Some combination of errors in pressure measurement, excitation voltage, or kinetic energy effects could reasonably account for the differences. At the same time, it is clear that the qualitative agreement between CRAFTI and the other methods is very good.

4.6 Conclusions

Measurements of the CRAFTI cross sections of the 20 biogenic amino acids yield results that, although not in absolute agreement with IMS measurements, correlate with the IMS measurements about as well as IMS measurements in different collision gases correlate with each other. The CRAFTI cross sections also correlate well with cross sections calculated from molecular models using the exact hard sphere scattering method, suggesting that the CRAFTI results accurately reflect differences in molecular structure and can be used to distinguish between proposed gas phase structures. In addition, the CRAFTI cross sections show nearly identical structural trends as are observed in IMS cross sections for the protonated amino acids. These observations provide strong evidence that CRAFTI can be used to obtain structurally meaningful data for gas phase ions. For the biogenic amino acids, the CRAFTI cross sections are also consistent with expectations about how compactly the various side chains should fold in the gas phase.

At this point the ability of CRAFTI to distinguish between structures of gas phase ions is roughly comparable to that of IMS for small molecules such as the protonated amino acids examined here. However, the CRAFTI technique is still in its infancy, and there is hope that further refinement of the technique may lead to improvements in accuracy and resolving power. In particular, the ability of CRAFTI to operate at various collision energies might be exploited to improve its performance; for instance, we suspect that the correlations between CRAFTI results and cross sections from IMS or from computed structures will probably improve if the CRAFTI experiments are conducted at constant kinetic energy in the center-of-mass reference frame. Further, it is likely that the resolving power of CRAFTI is collision energy-dependent and might be improved by judicious choice of collision energy. On the other hand, it is probable that the CRAFTI technique will fail at significantly higher molecular weights than were employed here,

because the assumption of single collision dephasing will eventually become invalid when the ions are much more massive than the collision gas. Although we have used CRAFTI in Ar successfully for *m/z* values up to about 1300, we do not know at what value of *m/z* the method is likely to fail. Experiments conducted at higher kinetic energies and in higher-field magnets than are available to us suggest measurements can be made for ions as massive as ubiquitin and cytochrome c.[2] Much work remains to be done.

4.7 References

1. (a) Yang, F.; Voelkel, J.; Dearden, D. V., Collision Cross Sectional Areas from Analysis of Fourier Transform Ion Cyclotron Resonance Line Width: A New Method for Characterizing Molecular Structure. *Anal. Chem.* **2012,** *84* (11), 4851-4857; (b) Yang, F.; Jones, C. A.; Dearden, D. V., Effects of Kinetic Energy and Collision Gas on Measurement of Cross Sections by Fourier Transform Ion Cyclotron Resonance Mass Spectrometry. *Int. J. Mass Spectrom.* **2015,** *378*, 143-150.

2. Mao, L.; Chen, Y.; Xin, Y.; Zheng, L.; Kaiser, N. K.; Marshall, A. G.; Xu, W., Collision Cross Section Measurements for Biomolecules within a High-Resolution Fourier Transform Ion Cyclotron Resonance Cell. *Anal. Chem.* **2015,** *87* (8), 4072-4075.

3. (a) Asbury, G. R.; Hill, H. H., Separation of amino acids by ion mobility spectrometry. *J. Chrom. A* **2000,** *902*, 433-437; (b) Beegle, L. W.; Kanik, I.; Matz, L.; Hill, H. H. J., Electrospray Ionization High Resolution Ion Mobility Spectrometry for the Detecton of Organic Compounds, 1. Amino Acids. *Anal. Chem.* **2001,** *73* (13), 3028-3034; (c) Bramwell, C. J.; Colgrave, M. L.; Creaser, C. S.; Dennis, R., Development and evaluation of a nano-electrospray ionisation source for atmospheric pressure ion mobility spectrometry. *Analyst* **2002,** *127*, 1467-1470.

4. Knapman, T. W.; Berryman, J. T.; Campuzano, I.; Harris, S. A.; Ashcroft, A. E., Considerations in experimental and theoretical collision cross-section measurements of small molecules using travelling wave ion mobility spectrometry-mass spectrometry. *Int. J. Mass Spectrom.* **2010,** *298* (1–3), 17-23.

5. Johnson, P. V.; Kim, H. I.; Beegle, L. W.; Kanik, I., Electrospray Ionization Ion Mobility Spectrometry of Amino Acids: Ion Mobilities and a Mass-Mobility Correlation. *J. Phys. Chem. A* **2004,** *108* (27), 5785-5792.

6. Jones, C. A.; Dearden, D. V., Linewidth Pressure Measurement: a New Technique for High Vacuum Characterization. *J. Am. Soc. Mass Spectrom.* **2015,** *26* (2), 323-329.

7. (a) Senko, M. W.; Canterbury, J. D.; Guan, S.; Marshall, A. G., A High-performance Modular Data System for Fourier Transform Ion Cyclotron Resonance Mass Spectrometry. *Rapid Commun. Mass Spectrom.* **1996,** *10* (14), 1839-1844; (b) Blakney, G. T.; Hendrickson, C. L.; Quinn, J. P.; Marshall, A. G. In *New Hardware for Ultrahigh Resolution and/or Data-Dependent SWIFT Ion Isolation in an FT-ICR Mass Spectrometer*, 56th ASMS Conference on Mass Spectrometry and Allied Topics, Denver, CO, June 1-5; Denver, CO, 2008; (c) Blakney, G. T.; Hendrickson, C. L.; Marshall, A. G., Predator data station: A fast data acquisition system for advanced FT-ICR MS experiments. *Int. J. Mass Spectrom.* **2011,** *306* (2), 246-252.

8. (a) Sievers, H. L.; Grützmacher, H.-F.; Caravatti, P., The geometrical factor of infinitely long cylindrical ICR cells for collision energy-resolved mass spectrometry: appearance energies of EI_2^+ (E=P, As, Sb, and Bi) from collision-induced dissociation of EI_3^+ and $[EI\bullet ligand]^+$ complexes. *Int. J. Mass Spectrom. Ion Processes* **1996,** *157/158*, 233-247; (b) Caravatti, P.; Allemann, M., The 'Infinity Cell': a New Trapped-ion Cell With Radiofrequency Covered

Trapping Electrodes for Fourier Transform Ion Cyclotron Resonance Mass Spectrometry. *Org. Mass Spectrom.* **1991,** *26*, 514-518.

9. Wigger, M.; Nawrocki, J. P.; Watson, C. H.; Eyler, J. R.; Benner, S. A., Assessing Enzyme Substrate Specificity Using Combinatorial Libraries and Electrospray Ionization Fourier Transform Ion Cyclotron Resonance Mass Spectrometry. *Rapid Commun. Mass Spectrom.* **1997,** *11* (16), 1749-1752.

10. Jiao, C. Q.; Ranatunga, D. R. A.; Vaughn, W. E.; Freiser, B. S., A Pulsed-Leak Valve for Use with Ion Trapping Mass Spectrometers. *J. Am. Soc. Mass Spectrom.* **1996,** *7* (1), 118-122.

11. Phelps, A. V., Cross Sections and Swarm Coefficients for Nitrogen Ions and Neutrals in N_2 and Argon Ions and Neutrals in Ar for Energies from 0.1 eV to 10 keV. *J. Phys. Chem. Ref. Data* **1991,** *20* (3), 557-573.

12. Chen, L.; Wang, T.-C. L.; Ricca, T. L.; Marshall, A. G., Phase-Modulated Stored Waveform Inverse Fourier Transform Excitation for Trapped Ion Mass Spectrometry. *Anal. Chem.* **1987,** *59*, 449-454.

13. (a) Shvartsburg, A. A.; Pederson, L. A.; Hudgins, R. R.; Schatz, G. C.; Jarrold, M. F., Structures of the Clusters Produced by Laser Desorption of Fullerenes: [2 + 2] Cycloadducts of Preshrunk Cages. *J. Phys. Chem. A* **1998,** *102* (41), 7919-7923; (b) Shvartsburg, A. A.; Hudgins, R. R.; Dugourd, P.; Jarrold, M. F., Structural Elucidation of Fullerene Dimers by High-Resolution Ion Mobility Measurements and Trajectory Calculation Simulations. *J. Phys. Chem. A* **1997,** *101* (9), 1684-1688; (c) Shvartsburg, A. A.; Jarrold, M. F., An exact hard-spheres scattering model for the mobilities of polyatomic ions. *Chem. Phys. Lett.* **1996,** *261* (1-2), 86-91; (d) Mesleh, M. F.; Hunter, J. M.; Shvartsburg, A. A.; Schatz, G. C.; Jarrold, M. F., Structural Information from Ion

Mobility Measurements: Effects of the Long Range Potential. *J. Phys. Chem.* **1996,** *100*, 16082-16086.

14. (a) Clemmer, D. E.; Jarrold, M. F., Ion Mobility Measurements and their Applications to Clusters and Biomolecules. *J. Mass Spectrom.* **1997,** *32* (6), 577-592; (b) Clowers, B. H.; Dwivedi, P.; Steiner, W. E.; Hill, H. H.; Bendiak, B., Separation of Sodiated Isobaric Disaccharides and Trisaccharides Using Electrospray Ionization-Atmospheric Pressure Ion Mobility-Time of Flight Mass Spectrometry. *J. Am. Soc. Mass Spectrom.* **2005,** *16* (5), 660-669.

15. Guan, S.; Li, G.-Z.; Marshall, A. G., Effect of Ion-Neutral Collision Mechanism on Trapped-Ion Equation of Motion: A New Mass Spectral Line Shape for High-Mass Trapped Ions. *Int. J. Mass Spectrom. Ion Proc.* **1997,** *167*, 185-193.

16. Guo, D.; Xin, Y.; Li, D.; Xu, W., Collision cross section measurements for biomolecules within a high-resolution FT-ICR cell: theory. *Phys. Chem. Chem. Phys.* **2015,** *17* (14), 9060-9067.

17. Marshall, A. G.; Hendrickson, C. L.; Jackson, G. S., Fourier Transform Ion Cyclotron Resonance Mass Spectrometry: A Primer. *Mass Spectrom. Rev.* **1998,** *17* (1), 1-35.

Chapter 5 **Relative alkali metal binding strengths of cryptands in the gas phase using SORI-CID.**

5.1 Abstract

We investigated solvent-free, gas phase complexes of alkali metal cations with novel cryptands: dimethyloxacryptands [3.3.3] and [3.3.4] and nitrogen cryptand [2.2.2] using electrospray Fourier transform ion cyclotron resonance mass spectrometry and collision induced dissociation techniques. All the cryptands readily form singly charged 1:1 metal: cryptand complexes. All complexes dissociate via loss of neutral cryptand and formation of positively charged metal ion. The data suggest that binding behavior for cryptand-metal complexes is a function of size selectivity and polarizability of host and guest in the gas phase. Cryptand [2.2.2] was the most effective binding agent for smaller cations like K^+ and Rb^+ but wasn't as effective as dimethyloxacryptand [3.3.4] and [3.3.3] for Cs^+. Dimethyloxacryptand [3.3.4] was found to bind all the metals better than its [3.3.3] analog.

5.2 Introduction

Cryptands are macrobicyclic host molecules that are formed by incorporating an extra ring to a crown ether. They are named using the form cryptand [x.y.z] where x, y and z represent the number of oxygens in each bridging arm of the ligand. They possess a cage-like structure and favorably encapsulate metals, anions and organic guests.[1] Cryptands have found several applications in the field of ion sensing,[2] supramolecular polymers,[3] molecular machines[4] and drug delivery.[5] This can be attributed to their unique three dimensional structure where the oxygen and nitrogen combine in a way which increases binding especially for spherically symmetric guests like alkali cations.[6] Indeed the binding selectivity and complex stability of cryptands exceeds that of crown ethers for selected ions,[7] ascribed to the geometry of crown ethers which reduces their

ability to bind effectively in such cases. This relatively enhanced binding ability of cryptands is termed the macrobicyclic cryptate effect.[6]

Utilizing a suitable host to selectively separate metal ions by forming a host guest complex is an active research area. One such application is the separation of radionuclides like ^{137}Cs and ^{90}Sr from nuclear waste for safe disposal.[8] Nitrogen-containing cryptands are well studied and their prior analysis with alkali metals has been achieved using several methods like X-ray crystallography,[9] NMR,[10] molecular dynamic methods[11] as well as gas phase studies.[12] However, there is still a need to develop host compounds with superior binding properties and hence newer synthesis of cryptands is aimed in this direction.

This study presents novel cryptands (Figure 5.1a, b) – dimethyloxacryptands (dmo cryptands) [3.3.3] and [3.3.4] which consist of two substituted methyl bridgehead carbon atoms connected by three bridges. The research objective of the present study is to investigate the binding energetics of these novel cryptands with alkali metals in terms of size selectivity in the gas phase and compare their performance with that of a well-known nitrogen containing cryptand [2.2.2]. The relative binding strengths and dissociation kinetics of cryptand-metal complexes are examined using variable energy Sustained off-resonance irradiation collision-induced dissociation (SORI-CID).

5.3 Experimental

5.3.1 Materials

Dimethyloxacryptands [3.3.3] and [3.3.4] and cryptand [2.2.2] were provided by IBC Advanced Technologies, Inc. (American Fork, UT) and used without further purification. Alkali metal salts (CsOH: Mallinckrodt, Paris, KY; KNO_3: Sigma-Aldrich, Milwaukee, WI; RbCl: Spectrum, Gardena, CA) were also used without further purification.

5.3.2 Sample preparation

Stock solutions of all the cryptands were prepared at about 4 mM concentration by dissolving the samples in methanol: water (50:50). Solutions for electrospray were prepared by mixing and diluting the stock solutions with 50:50 methanol: water so that the final concentration of cryptand was about 100 μM. Alkali metal salts were dissolved in water at 1 mM concentration and diluted in final solution to 300 μM.

5.3.3 Instrumentation

All experiments were done using a Fourier transform ion-cyclotron resonance mass spectrometer (Bruker model Apex 47e FT-ICR MS) equipped with a MIDAS PREDATOR data system (National High Magnetic Field Ion Cyclotron Resonance Facility; Tallahassee, FL).[13] Ions were generated in a microelectrospray source modified from an Analytica design, with a heated metal capillary drying tube based on the design of Eyler.[14] The source was typically operated at a flow rate of 30 μl/hr. All masses determined are within 1 ppm of masses calculated for the proposed formulas.

5.3.4 Sustained off-resonance irradiation collision-induced dissociation experiments

The stored waveform inverse Fourier transform (SWIFT) method was used to isolate the ion of interest.[15] SORI-CID experiments were carried out by irradiating 1 kHz above the resonant frequency of the target ion.[16] Argon was introduced as the collision gas using a Freiser-type pulsed leak valve.[17] SORI events included pulsing the Ar background pressure in the trapping cell up to

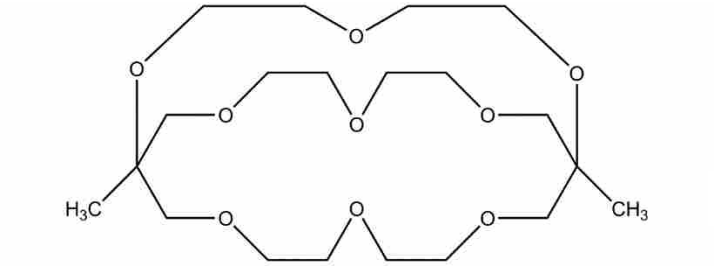

1,11-dimethyl-3,6,9,13,16,19,21,24,27-nonaoxabicyclo[9.9.7]heptacosane
Chemical Formula: $C_{20}H_{38}O_9$
Exact Mass: 422.25

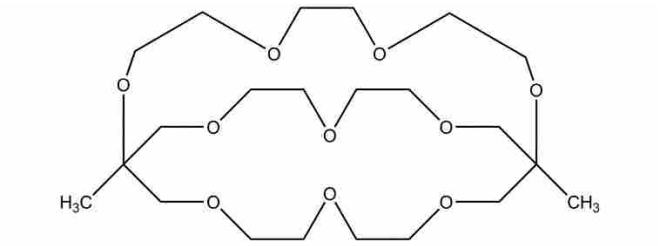

1,12-dimethyl-2,5,8,11,14,17,20,23,26,29-decaoxabicyclo[10.9.9]triacontane
Chemical Formula: $C_{22}H_{42}O_{10}$
Molecular Weight: 466.57

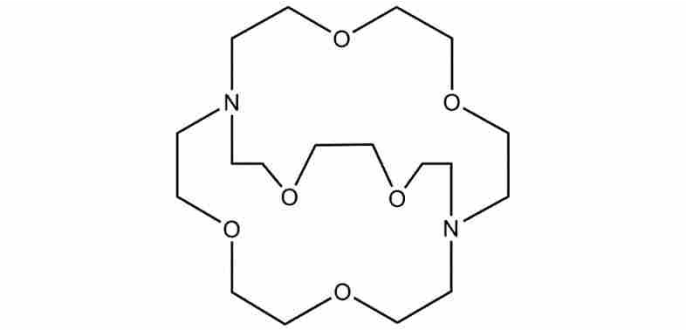

4,7,13,16,21,24-hexaoxa-1,10-diazabicyclo[8.8.8]hexacosane
Chemical Formula: $C_{18}H_{36}N_2O_6$
Molecular Weight: 376.49

Figure 5.1 Host ligands used in the study (a) dimethyloxacryptand [3.3.3] (b) dimethyloxacryptand [3.3.4] (c) cryptand [2.2.2]

10^{-5} mbar pressure, waiting 3s for conditions to fully stabilize and applying the off-resonance irradiation for a variable amount of time (which allows variation of the total energy deposited in the ions; herein, times ranged from 1 to about 500 ms, with amplitudes kept high and durations kept short to minimize radiative cooling between collisions), followed by a 5-s delay to allow the trapping cell to return to baseline pressure (about 10^{-9} mbar) prior to detection. Four scans were averaged for each SORI excitation duration.

5.3.5 Data analysis

Transient signals were analyzed using the Igor Pro software package (version 6.3.7.2; Wavemetrics, Lake Oswego, OR, USA). For SORI experiments, the Igor program was used to extract peak amplitudes for a set of spectra that differ in one or more experimental parameters and followed by generation of tables of peak intensities as a function of SORI excitation duration. The resulting parent and product ion peak intensities were normalized against total ion signal, and the relative SORI collision energy was scaled to account for differences in mass, excitation amplitude (although most experiments were conducted while maintaining a constant excitation amplitude) and pressure. Relative SORI energies were calculated as described previously.[18] Energies obtained from these experiments may be compared qualitatively, but are not quantitative due to uncertainties about the absolute kinetic energies of the colliding partners and conversion efficiency from kinetic to internal energy.

5.4 Results

5.4.1 Electrospray of cryptands with alkali metals

The alkali metals and cryptand ligands were electrosprayed and Fourier transform ion cyclotron mass spectrometry was performed. Metal-ligand 1:1 complexes were observed for all

combinations of alkali metal cation with ligand dmo cryptands [3.3.3], [3.3.4] and cryptand [2.2.2].

5.4.2 Dissociation behavior of cryptand-alkali metal complexes

SORI–CID experiments were performed on 1:1 complexes, [cryptand+M]$^+$. All the complexes demonstrate one primary dissociation pathway: loss of neutral cryptand yielding positively charged metal cation (Figure 5.2). The average energy that can be deposited during a SORI event, E_{SORI} was calculated using Equation 5-1:[18]

$$E_{SORI} \propto N^* \sigma\, t_{coll} \left(\frac{M}{M+m}\right) \frac{{V_{pp}}^3}{m^2} \qquad (5\text{-}1)$$

Where N^* is the neutral gas number density, M is the mass of the neutral, m is the mass of the ion, and V_{pp} is the peak-to-peak amplitude of the SORI excitation pulse, t_{coll} is the length of the SORI event and σ is collision cross section. For simplification of the calculations, the collision cross sections for all the complexes being compared were assumed to be similar and hence omitted from the Equation 5-1 for the determination of relative E_{SORI} energies. An example showing the dissociation product of [dmo cryptand 333+Cs]$^+$ is given in Figure 5.3, where the relative signal abundance of the parent ion and product ions are plotted against the relative SORI dissociation energies.

The disappearance curves of the parent ions are plotted against the relative E_{SORI} energies, as shown in Figure 5.4. The falling portion of the dissociation curves suggest that the dissociation threshold energies decrease as the metal radius increase. Hence, the smallest metal in the study, K^+, is the most strongly bound by all the cryptands followed by Rb^+ and Cs^+. $E_{SORI,50}$ represents the relative energies for 50% loss of the parent ion and was calculated by linear fitting of the falling

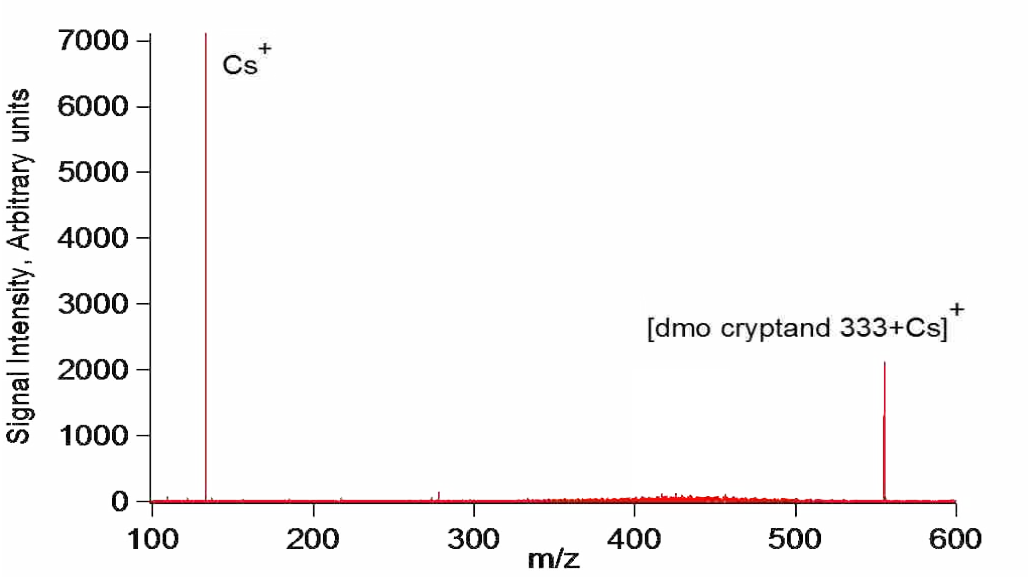

Figure 5.2 Dissociation spectra of [dmo cryptand 333+Cs]$^+$ showing loss of neutral cryptand.

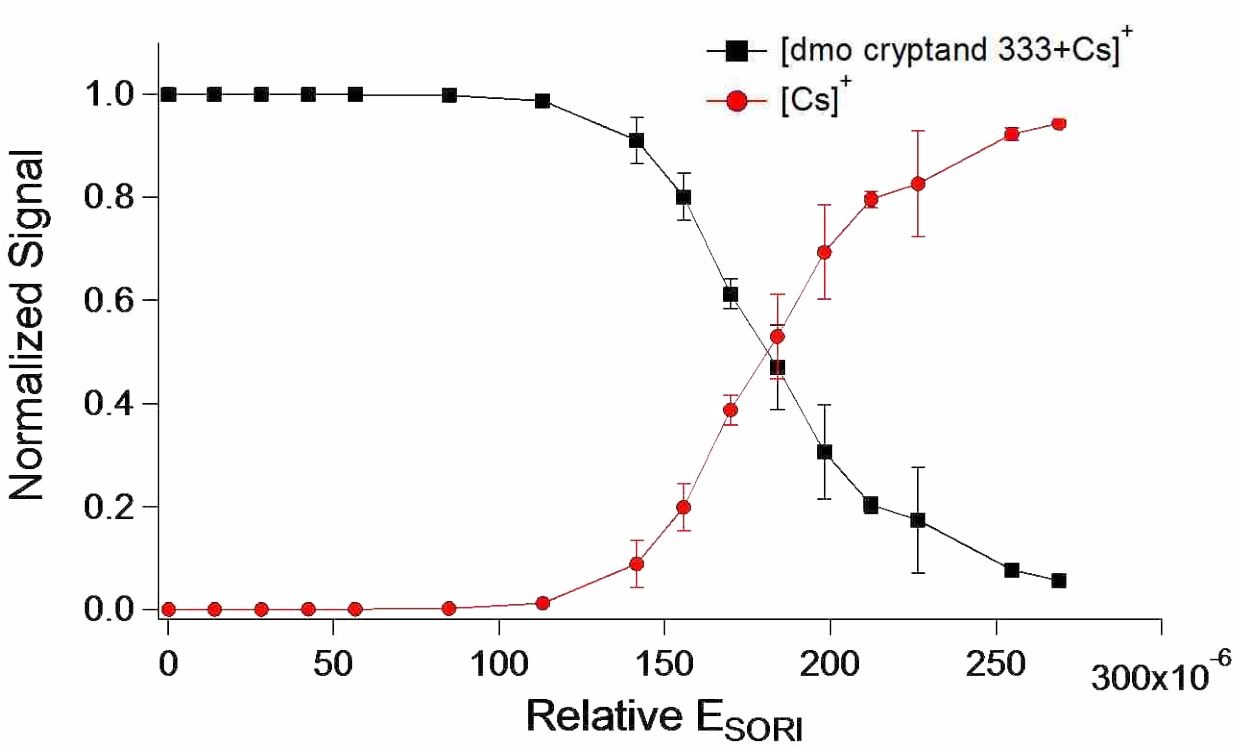

Figure 5.3 SORI ion yield curves for [dmo cryptand 333+Cs]$^+$ complex.

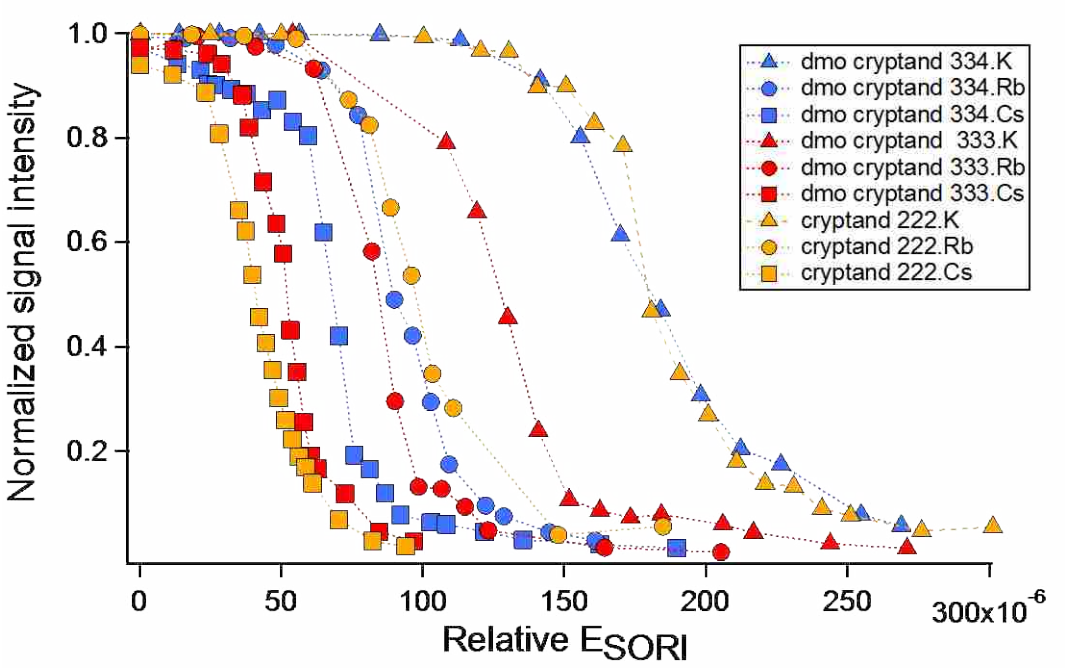

Figure 5.4 SORI parent ion survival curve for metal-cryptand complexes as a function of average collision energy

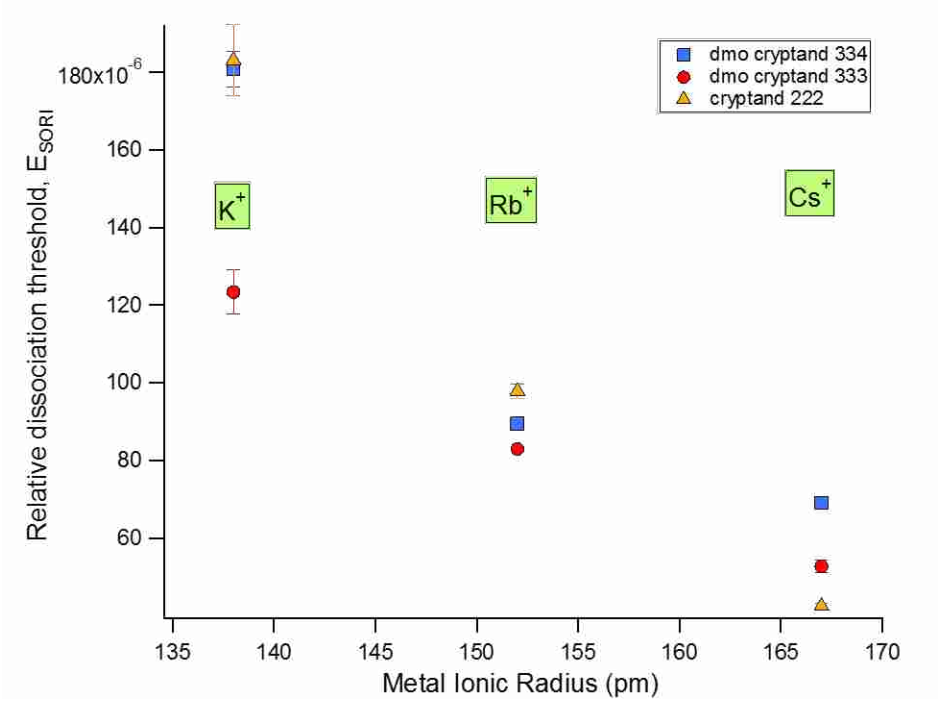

Figure 5.5 Variation of dissociation threshold energy as a function of metal ion radius

portion of each disappearance curve in Figure 5.4. It indicates the overall stability for each complex and is plotted for all the cryptand-metal complexes as a function of guest metal ion radius (Figure 5.5). The graph suggests that the relative binding with the guest metals K^+ and Rb^+ is strongest for cryptand [2.2.2] followed by dmo cryptands [3.3.4] and [3.3.3]. But interestingly when the guest metal is Cs^+, the dmo cryptand [3.3.4] binds Cs^+ the strongest followed by dmo cryptand [3.3.3] and cryptand [2.2.2].

5.5 Discussion

The binding of alkali metal cations to cryptands follows the gas phase behavior observed earlier for crown ethers.[19] The electrostatic interactions between the cation and donor oxygen or nitrogen atoms in the cryptand govern the binding behavior in the gas phase. The strongest binding in all the cryptands is observed for the small, charge dense metals like K^+, which act as effective polarizers, leading to formation of a stronger interaction. The weakest binding is observed for the larger, more diffuse cations, like Cs^+, which act as weak polarizers for each of the ligands. While comparing complexes of dmo cryptands [3.3.3] and [3.3.4] with the same guest, the observation of the trend for binding energies dmo [3.3.4] > dmo [3.3.3] can be explained based on two factors. The most important factor is the relative polarizability of the host ligand. Polarizability of the host ligand critically impacts the strength of the ion-neutral interactions and thus the binding energy.[20] The polarizabilities increase with the size and number of substituents.[21] Therefore, the larger dmo cryptand [3.3.4] has greater intrinsic dissociation energies than the smaller dmo crpytand [3.3.3]. The second factor is related to the dissociation kinetics of these complexes. Addition of more substituted groups lends greater internal degrees of freedom to the complex, which can result in distribution of collision energy prior to causing dissociation. This can lead to effective slowing of the dissociation kinetics for the larger cryptand complexes. Hence, more energy would be needed

for dissociating larger complexes at the same rate relative to less substituted ones. These effects explain the greater dissociation energy observed for the larger dmo cryptand [3.3.4] relative to the smaller one [3.3.3]. However, considering the long dissociation times needed for SORI the impact of additional degrees of freedom can be hypothesized to be low. Therefore, polarizability effects probably dominate the observed dissociation behavior and binding strengths measured by $E_{SORI,50}$.

Literature evidence shows that cryptand [2.2.2] forms 'inclusive' complexes with small alkali cations.[9, 12, 22] It is highly selective for small cations where the cations fit within the cavity easily, leading to observation of stronger complexes. Hence, cations which are small enough to enter the cavity are effectively encapsulated but a larger cation like Cs^+ fails to go into the [2.2.2] cavity and sits on the outside of the binding cavity of the ligand.[12] Hence a crossover in the relative binding preference is observed for dmo cryptands and [2.2.2] when the cation size becomes larger than the cryptand cavity. It is postulated that the metal preferentially binds on the face of the smaller ligands for greater contact with donor groups.[12] The dmo cryptand [3.3.3] may be too large to bind K^+ and could be a better size match for the Cs^+, but binds weakly in comparison to [3.3.4] due to dominant polarizability effects explained earlier.

Gas phase structural determination offers advantages over equivalent studies in solution. The primary motivation behind gas phase studies is observation of molecular interaction in the absence of solvent interference. The most important effect exerted by the solvent is dissolution whereby the intrinsic affinity and solvation energies of the host and guest species need to be accounted for. From a thermodynamic perspective, there are differences in entropic compensation involving a host-guest complexation. Entropic effects are expected to be greater in solution than in the gas phase. Solvation of an ion or a ligand involves order in many solvent molecules, much of which is lost when the guest ion binds to the host and solvent is displaced. This explains a lot

of the so-called “hydrophobic effects” seen in condensed phase. In the gas phase, the only entropic changes are those associated with only the guest binding the host and the subsequent loss of degrees of freedom. Highly charged small metal ions acquire a much greater effective ionic radius by attracting solvent molecules. This would impact both entropy and the net change in size and gas phase results would be expected to be very different from solution phase. However, as the size of the metal increases, interaction with the solvent decreases and effective ionic radius in solution does not change significantly relative to that observed for the smaller ion. Thus, as the metal size increases, one would expect the difference in gas and solution phase results to decrease. This augurs well for the Cs binding cryptands, whose efficacy would be expected to translate into the solution phase for practical applications like nuclear waste removal.

5.6 Conclusions

Studies on the gas phase chemistry of alkali metal-cryptand complexes revealed size and host/guest polarizability to be the most critical factors governing complex formation and stability. The charge density of metals affects the binding similar to what is observed for crown ether-metal complexes. The stability of the cryptand-alkali metal complexes, as judged by SORI dissociation thresholds, decreases as the cation size increases from K^+ to Cs^+. This behavior is attributed to the fact that the smaller metal ions are more effective polarizers and hence the bond strength decreases as the alkali metals become larger and poorer polarizers. Dmo cryptand [3.3.4]-M+ complexes are stronger relative to [3.3.3]-M+ complex, as larger ligands are more effective polarizers. Cryptand [2.2.2] is size selective for smaller guests while dmo cryptand [3.3.4] is selective for Cs^+ which can have potential applications for nuclear waste removal. All these results offer basic understanding for future investigation of host-guest interactions involving cryptand ligands.

5.7 References

1. (a) Izatt, R. M.; Pawlak, K.; Bradshaw, J. S.; Bruening, R. L., Thermodynamic and kinetic data for macrocycle interactions with cations and anions. *Chem. Rev.* **1991,** *91* (8), 1721-2085; (b) Kang, S. O.; Llinares, J. M.; Day, V. W.; Bowman-James, K., Cryptand-like anion receptors. *Chem. Soc. Rev.* **2010,** *39* (10), 3980-4003; (c) Han, Y.; Jiang, Y.; Chen, C.-F., Cryptand-based hosts for organic guests. *Tetrahedron* **2015,** *71* (4), 503-522.

2. Woiczechowski-Pop, A.; Gligor, D.; Bende, A.; Varodi, C.; Bogdan, E.; Terec, A.; Grosu, I., Synthesis, structure, electrochemical behaviour and electrochemical investigations on the assembling with pyrene of a novel C3 cryptand. *Supramol. Chem.* **2015,** *27* (1-2), 52-58.

3. Zhang, M.; Xu, D.; Yan, X.; Chen, J.; Dong, S.; Zheng, B.; Huang, F., Self-Healing Supramolecular Gels Formed by Crown Ether Based Host–Guest Interactions. *Angew. Chem.* **2012,** *124* (28), 7117-7121.

4. Caputo, C. B.; Zhu, K.; Vukotic, V. N.; Loeb, S. J.; Stephan, D. W., Cover Picture: Heterolytic Activation of H2 Using a Mechanically Interlocked Molecule as a Frustrated Lewis Base (Angew. Chem. Int. Ed. 3/2013). *Angew. Chem. Int. Ed.* **2013,** *52* (3), 773-773.

5. Ito, T.; Yamaguchi, T., Osmotic pressure control in response to a specific ion signal at physiological temperature using a molecular recognition ion gating membrane. *J. Am. Chem. Soc.* **2004,** *126* (20), 6202-6203.

6. Lehn, J.; Sauvage, J., Cryptates. XVI.[2]-Cryptates. Stability and selectivity of alkali and alkaline-earth macrobicyclic complexes. *J. Am. Chem. Soc.* **1975,** *97* (23), 6700-6707.

7. Izatt, R. M.; Bradshaw, J. S.; Nielsen, S. A.; Lamb, J. D.; Christensen, J. J.; Sen, D., Thermodynamic and kinetic data for cation-macrocycle interaction. *Chem. Rev.* **1985,** *85* (4), 271-339.

8. (a) Ali, S. M., Design and screening of suitable ligand/diluents systems for removal of Sr 2+ ion from nuclear waste: Density functional theoretical modelling. *Comp. Theor. Chem.* **2014,** *1034*, 38-52; (b) Awual, M. R.; Suzuki, S.; Taguchi, T.; Shiwaku, H.; Okamoto, Y.; Yaita, T., Radioactive cesium removal from nuclear wastewater by novel inorganic and conjugate adsorbents. *Chem. Eng. J.* **2014,** *242*, 127-135.

9. Dobler, M., Ionosphores and their structures. **1981**.

10. Kauffmann, E.; Dye, J. L.; Lehn, J. M.; Popov, A. I., A study of the inclusive and exclusive cesium cryptates in nonaqueous solvents by cesium-133 NMR. *J. Am. Chem. Soc.* **1980,** *102* (7), 2274-2278.

11. Troxler, L.; Wipff, G., Conformation and dynamics of 18-crown-6, cryptand 222, and their cation complexes in acetonitrile studied by molecular dynamics simulations. *J. Am. Chem. Soc.* **1994,** *116* (4), 1468-1480.

12. Chen, Q.; Cannell, K.; Nicoll, J.; Dearden, D. V., The macrobicyclic cryptate effect in the gas phase. *J. Am. Chem. Soc.* **1996,** *118* (27), 6335-6344.

13. Blakney, G. T.; Hendrickson, C. L.; Marshall, A. G., Predator data station: A fast data acquisition system for advanced FT-ICR MS experiments. *Int. J. Mass spectrom.* **2011,** *306* (2), 246-252.

14. Wigger, M.; Nawrocki, J. P.; Watson, C. H.; Eyler, J. R.; Benner, S. A., Assessing enzyme substrate specificity using combinatorial libraries and electrospray ionization-Fourier transform ion cyclotron resonance mass spectrometry. *Rapid Commun. Mass Spectrom.* **1997,** *11*, 1749-1752.

15. Chen, L.; Wang, T. C. L.; Ricca, T. L.; Marshall, A. G., Phase-modulated stored waveform inverse Fourier transform excitation for trapped ion mass spectrometry. *Anal. Chem.* **1987,** *59* (3), 449-454.

16. Gauthier, J.; Trautman, T.; Jacobson, D., Sustained off-resonance irradiation for collision-activated dissociation involving Fourier transform mass spectrometry. Collision-activated dissociation technique that emulates infrared multiphoton dissociation. *Anal. Chim. Acta* **1991,** *246* (1), 211-225.

17. Jiao, C. Q.; Ranatunga, D. R. A.; Vaughn, W. E.; Freiser, B. S., A pulsed-leak valve for use with ion trapping mass spectrometers. *J. Am. Soc. Mass Spectrom.* **1996,** *7* (1), 118-122.

18. Zhang, H.; Ferrell, T. A.; Asplund, M. C.; Dearden, D. V., Molecular beads on a charged molecular string: α, ω-alkyldiammonium complexes of cucurbit [6] uril in the gas phase. *Int. J. Mass spectrom.* **2007,** *265* (2), 187-196.

19. More, M. B.; Ray, D.; Armentrout, P., Intrinsic affinities of alkali cations for 15-crown-5 and 18-crown-6: bond dissociation energies of gas-phase M+-crown ether complexes. *J. Am. Chem. Soc.* **1999,** *121* (2), 417-423.

20. Su, T.; Bowers, M., Gas Phase Ion Chemistry. *by MT Bowers, Academic, New York* **1979**.

21. Miller, K. J.; Savchik, J., A new empirical method to calculate average molecular polarizabilities. *J. Am. Chem. Soc.* **1979,** *101* (24), 7206-7213.

22. Wipff, G.; Kollman, P., Molecular mechanical calculations on a macrocyclic receptor: the 222 cryptand and its alkali complexes. *Nouveau journal de chimie* **1985,** *9* (7), 457-465.

Chapter 6 Summary and Perspective

A holistic molecular description of both structure and conformation is of rapidly growing importance in the fields of chemistry and medicine. This dissertation explores a novel FTICR-MS based method for measuring conformation termed "CRAFTI" and investigates different molecular systems to demonstrate how CRAFTI can be used to gain structural insights.

In **Chapter 3**, CRAFTI was applied to crown ether – alkylmonoamine complexes. The results highlighted the analytical sensitivity of CRAFTI towards changes in crown ether ring size and alkylammonium chain length. The extreme analytical sensitivity of CRAFTI was further demonstrated by distinguishing crown ether complexes of the normal and branched structural isomers of butylamine. The results were further compared with (a) the existing "gold standard" method for conformation determination, ion mobility spectrometry (IMS), and (b) *in silico* determinations from molecular mechanics. Even though point to point overlap of absolute vales was not achieved, strong linear correlations between the methods offer a proof of concept for CRAFTI which could be further utilized for validation and calibration.

Evaluation of the 20 biogenic amino acids in **Chapter 4** was undertaken using CRAFI to sample a broader range of molecules. The experimental findings were found to be reasonably well correlated with both IMS determinations, and those computed using hard sphere scattering computational methods. For the biogenic amino acids, the CRAFTI cross sections are also consistent with expectations about how compactly the various side chains should fold in the gas phase. This suggests that CRAFTI can accurately reflect differences in molecular structure and can hence be utilized to distinguish between proposed structures from computation. Protonated amino acids evaluated using CRAFTI and IMS displayed identical structural trends. These

evidences make CRAFTI a promising method to obtain relevant structural information for gas phase ions.

In an effort directed towards comprehensive molecular characterization, binding energetics of host guest complexes where evaluated using SORI-CID in **Chapter 5**. Cryptands and alkali metal ions were chosen as host and guest respectively. The complex formation and stability was found to be strongly size dependent. This was inferred from progressive decrease in SORI dissociation thresholds as the guest ion size decreased from K^+ to Cs^+. Polarizability decreases with increased size of the metal ions and hence the bond strength decreases for increasing metal ion size. For a given metal ion, increasing the cryptand size from [3.3.3]-M^+ to [3.3.4]-M^+ increased the complex strength as larger ligands are more effective polarizers.

The current dissertation demonstrates the analytical sensitivity and versatility of CRAFTI, which shows enormous promise especially for biochemical applications. However, there is still some way before CRAFTI fulfils its promise and becomes a routine technique for conformation measurement. Three specific areas deserve further attention:

(a) One major area would be finding the upper mass limit for CRAFTI. Although we have used CRAFTI in Ar successfully for m/z values up to about 1300, we do not know at what value of m/z the method is likely to fail. Experiments conducted at higher kinetic energies and in higher-field magnets than are available to us suggest measurements can be made for ions as massive as ubiquitin and cytochrome c. The simplest way to do this is to incrementally increase the mass of ions being analyzed by CRAFTI. It will be important to know whether the upper m/z limit will be able to accommodate peptides and small proteins in our 4.7 T FTICR-MS. We expect that as this limit is reached the linewidths plotted as a function of pressure will become

non-linear. This will happen because single collisions will no longer be energetic enough to dephase the ions. The limit could be increased by increasing the magnetic field strength or by using heavier neutral collision gas.

(b) Another area would be using the high resolution of FTICR-MS to an advantage when calculating CCS. One of the key experiments would be measuring cross sections for multiply charged multimers. The objective of these experiments is to find what happens when ions with the same m/z but different cross sections are present in the cell at the same time. In drift ion mobility, such multimers are separated according to mobility and multiple peaks are observed. In CRAFTI there is no physical separation and it is unclear whether we would be able to distinguish between the different cross sections. Due to the high resolution of FTICR-MS we can easily see the isotope pattern to discern the charge state of the ion. Amino acids are known to make multiply charged clusters in the gas phase and hence CCS for such clusters should be observed in theory. It would be interesting to make these gas phase complexes and evaluate them using CRAFTI.

(c) Simultaneous measurement of CCS for multiple ions is another future investigation area. As all the species would be subjected to same pressure and excitation waveform conditions, such measurements through a multi-CRAFTI procedure will enable simultaneous structural comparison of multiple ions. Some preliminary work in this regard has been done where software for defining and generating multi-frequency excitation waveforms (consisting of summed sine waves) was written using LabVIEW 2013 (National Instruments; Austin, TX). The systems studied so far are small supramolecular complexes like the macrocyclic ligand 12-crown-4 (12C4) with Na^+: CCS for both $(12C4)Na^+$ (m/z 199) and $(12C4)_2Na^+$ (m/z 375) were observed. The results are very encouraging and we see good agreement between cross

sections measured using single-frequency excitation and those measured using simultaneous excitation of both resonant frequencies. Further studies should be conducted on systems like biomolecules and other examples from ion mobility which have been investigated thoroughly before. The new technique offers the possibility of more accurate relative cross section measurements as well as allowing the use of an internal calibrant ion in CCS measurements.